INSTITUTO LATINO-AMERICANO DE CIÊNCIAS DA VIDA E DA NATUREZA (ILACVN)

ENGENHARIA FÍSICA

AUTOMATIC TEMPERATURE EXTRACTION FROM ARRESTERS' THERMAL IMAGES WITH ARTIFICIAL INTELLIGENCE

ADEL ABDUL KARIM MOUSSA

Foz do Iguaçu
2023

INSTITUTO LATINO-AMERICANO DE CIÊNCIAS DA VIDA E DA NATUREZA (ILACVN)

ENGENHARIA FÍSICA

AUTOMATIC TEMPERATURE EXTRACTION FROM ARRESTERS' THERMAL IMAGES WITH ARTIFICIAL INTELLIGENCE

ADEL ABDUL KARIM MOUSSA

Trabalho de Conclusão de Curso apresentado ao Instituto Latino-Americano de Ciências da Vida e da Natureza da Universidade Federal da Integração Latino-Americana, como requisito parcial à obtenção do título de Bacharel em Engenharia Física.

Orientador: Prof. Dr. Joylan Nunes Maciel
Co-orientador: Jhoan Rodrigo Perez Vargas

Foz do Iguaçu
2023

ADEL ABDUL KARIM MOUSSA

AUTOMATIC TEMPERATURE EXTRACTION FROM ARRESTERS' THERMAL IMAGES WITH ARTIFICIAL INTELLIGENCE

Trabalho de Conclusão de Curso apresentado ao Instituto Latino-Americano de Ciências da Vida e da Natureza da Universidade Federal da Integração Latino-Americana, como requisito parcial à obtenção do título de Bacharel em Engenharia Física.

BANCA EXAMINADORA

gov.br Documento assinado digitalmente
JOYLAN NUNES MACIEL
Data: 17/06/2023 12:42:24-0300
Verifique em https://validar.iti.gov.br

_____
Orientador: Prof. Dr. Joylan Nunes Maciel
UNILA

_____
Prof. Dr. Marcelo Honnicke
UNILA

_____
Prof. Dr. Willian Zalewski
UNILA

_____
Prof. Dr. Marcelo Nepomuceno Kapp
UNILA

Foz do Iguaçu, 02 de junho de 2023.

TERMO DE SUBMISSÃO DE TRABALHOS ACADÊMICOS

Nome completo do autor(a):_____

_____

Curso: _____

	Tipo de Documento
(…..) graduação	(…..) artigo
(…..) especialização	(…..) trabalho de conclusão de curso
(…..) mestrado	(…..) monografia
(…..) doutorado	(…..) dissertação
	(…..) tese
	(…..) CD/DVD – obras audiovisuais
	(…..) _____

Título do trabalho acadêmico: _____

_____

_____

Nome do orientador(a): _____

Data da Defesa: _____/_____/_____

Licença não-exclusiva de Distribuição

O referido autor(a):

a) Declara que o documento entregue é seu trabalho original, e que o detém o direito de conceder os direitos contidos nesta licença. Declara também que a entrega do documento não infringe, tanto quanto lhe é possível saber, os direitos de qualquer outra pessoa ou entidade.

b) Se o documento entregue contém material do qual não detém os direitos de autor, declara que obteve autorização do detentor dos direitos de autor para conceder à UNILA – Universidade Federal da Integração Latino-Americana os direitos requeridos por esta licença, e que esse material cujos direitos são de terceiros está claramente identificado e reconhecido no texto ou conteúdo do documento entregue.

Se o documento entregue é baseado em trabalho financiado ou apoiado por outra instituição que não a Universidade Federal da Integração Latino-Americana, declara que cumpriu quaisquer obrigações exigidas pelo respectivo contrato ou acordo.

Na qualidade de titular dos direitos do conteúdo supracitado, o autor autoriza a Biblioteca Latino-Americana – BIUNILA a disponibilizar a obra, gratuitamente e de acordo com a licença pública *Creative Commons* **Licença 3.0 Unported.**

Foz do Iguaçu, _____ de _____ de _____.

_____

Assinatura do Responsável

Dedico este trabalho à minha família, que sempre foi minha fonte de apoio, incentivo e inspiração ao longo de minha jornada acadêmica. Sua crença em mim e seus sacrifícios me possibilitaram alcançar este importante marco.

AGRADECIMENTOS

Em primeiro lugar, gostaria de expressar minha mais profunda gratidão à minha família por seu amor incondicional, apoio e encorajamento ao longo da minha jornada acadêmica. Vocês são a minha fonte de inspiração e força.

Agradeço ao meu professor orientador, pelo seu tempo, paciência e orientação constante neste trabalho. Sua experiência e conhecimento foram essenciais para o desenvolvimento deste projeto, e sou grato por ter tido a oportunidade de aprender com você.

Aos professores da banca, gostaria de agradecer pelas suas valiosas sugestões, críticas construtivas e orientações que enriqueceram este trabalho.

Aos meus amigos, agradeço o apoio emocional, as conversas inspiradoras e os momentos de descontração que tornaram esta jornada mais agradável. Vocês estiveram ao meu lado em momentos de desafios e celebrações e, por isso, serei sempre grato.

Aos colegas de curso, agradeço a colaboração, troca de ideias e amizade ao longo destes anos. Nós compartilhamos experiências e conhecimentos que contribuíram para nosso crescimento pessoal e profissional.

Por último, mas não menos importante, gostaria de agradecer a todos aqueles que, direta ou indiretamente, contribuíram para a realização deste trabalho. Cada um de vocês desempenhou um papel importante no meu desenvolvimento acadêmico, e sou grato por todas as lições aprendidas.

Nature does not hurry, yet everything is accomplished.
Lao Tzu

RESUMO

Os para-raios são fundamentais para garantir a confiabilidade, a economia e a segurança dos sistemas elétricos. Entretanto, a degradação que ocorre naturalmente ao longo do tempo representa um problema que leva a um desafio ainda em aberto, no qual vários estudos científicos propuseram e exploraram técnicas inovadoras de diagnóstico. Um novo método de diagnóstico manual está sendo empregado atualmente em subestações elétricas. O método emprega uma lógica anotada paraconsistente de dois valores, usando medições de temperatura por termografia infravermelha e dados de corrente de fuga resistiva como entrada para uma avaliação precisa da condição do para-raios. Tal método baseia-se em campanhas de coleta para obter imagens térmicas de para-raios de alta tensão em operação, exigindo posteriormente a extração manual dos dados de temperatura máxima e média e suas diferenças (delta) ao longo do eixo principal de cada para-raios por meio de um software de câmera digital. Nesse contexto, este estudo tem como objetivo aprimorar e automatizar o diagnóstico de para-raios por meio do cálculo automático da temperatura delta, introduzindo um novo método, cuja abordagem é baseada em Inteligência Artificial Deep Learning. O método proposto neste estudo emprega um modelo de Rede Neural Convolucional de Região de Máscara (Mask R-CNN) para segmentação dos para-raios a partir da imagem térmica, seguido de um algoritmo para extração de dados de temperatura dos para-raios, que são usados para diagnóstico de degradação. O processo de segmentação de para-raios com Mask R-CNN, em imagens térmicas, mostrou-se viável, com uma precisão média de 83,85%. A análise comparativa da precisão média entre o método manual (original) e o método proposto (automatizado), a partir de 195 imagens térmicas processadas, revelou um Erro Percentual Absoluto Médio (MAPE) de 11,48% na temperatura delta, que é usada na análise da degradação do para-raios. Esse resultado demonstra que o método proposto neste estudo é viável e permite automatizar a inspeção de para-raios. Investigações futuras consistem em refinar o processo de segmentação por meio do ajuste fino dos hiperparâmetros e do uso da técnica de validação cruzada.

Palavras-chave: para-raios; degradação; aprendizado profundo; extração de temperatura; imagens térmicas.

RESUMEN

Los pararrayos son fundamentales para garantizar la fiabilidad, economía y seguridad de los sistemas eléctricos. Sin embargo, la degradación que se produce de forma natural con el paso del tiempo representa un problema que plantea un reto aún abierto, en el que varios estudios científicos han propuesto y explorado técnicas de diagnóstico innovadoras. Actualmente se está empleando un nuevo método de diagnóstico manual en subestaciones eléctricas, el método emplea una lógica anotada paraconsistente de dos valores, utilizando medidas de temperatura de termografía infrarroja y datos de corriente de fuga resistiva como entrada para una evaluación precisa del estado del descargador de sobretensión. Dicho método se basa en campañas de recogida para obtener imágenes térmicas de pararrayos de alta tensión en funcionamiento, requiriendo posteriormente la extracción manual de los datos de temperatura máxima y media y sus diferencias (delta) a lo largo del eje principal de cada pararrayos mediante un software de cámara digital. En este contexto, este estudio pretende mejorar y automatizar el diagnóstico de pararrayos mediante el cálculo automatizado de la temperatura delta introduciendo un nuevo método, cuyo enfoque se basa en Deep Learning de Inteligencia Artificial. El método, propuesto en este estudio, emplea un modelo Mask Region - Convolutional Neural Network (Mask R-CNN) para la segmentación de los pararrayos a partir de la imagen térmica, seguido de un algoritmo para la extracción de los datos de temperatura de los pararrayos, que se utilizan para el diagnóstico de la degradación. El proceso de segmentación de pararrayos con Mask R-CNN, en imágenes térmicas, demostró ser viable, con una precisión media del 83,85%. El análisis comparativo de la precisión media entre el método manual (original) y el método propuesto (automatizado), a partir de 195 imágenes térmicas procesadas, reveló un Error Porcentual Absoluto Medio (MAPE) del 11,48% en la temperatura delta, que se utiliza en el análisis de la degradación del pararrayos. Este resultado demuestra que el método propuesto en este estudio es viable y permite automatizar la inspección de pararrayos. Futuras investigaciones consisten en refinar el proceso de segmentación afinando los hiperparámetros y utilizando la técnica de validación cruzada.

Palabras clave: pararrayos; diagnóstico; degradación; aprendizaje profundo; extracción de temperatura.

ABSTRACT

Lightning arresters are fundamental to ensure the reliability, economy, and safety of electrical systems. However, the degradation that occurs naturally over time represents a problem that leads to a still open challenge, where several scientific studies have proposed and explored innovative diagnostic techniques. A new manual diagnostic method is currently being employed in electrical substations, the method employs two-valued paraconsistent annotated logic, using infrared thermography temperature measurements and resistive leakage current data as input for accurate assessment of surge arrester condition. Such a method is based on collection campaigns to obtain thermal images of operating high-voltage lightning arresters, subsequently requiring the manual extraction of the maximum and average temperature data and their differences (delta) along the main axis of each arrester by means of a digital camera software. In this context, this study aims to improve and automate the diagnosis of lightning arresters through the automated calculation of the delta temperature by introducing a new method, whose approach is based on Artificial Intelligence Deep Learning. The method, proposed in this study, employs a Mask Region - Convolutional Neural Network (Mask R-CNN) model for segmentation of the lightning rods from thermal image, followed by an algorithm for extraction of temperature data from the lightning rods, which are used for degradation diagnosis. The lightning rod segmentation process with Mask R-CNN, on thermal images, proved to be feasible, with an average accuracy of 83.85%. The comparative analysis of the average accuracy between the manual method (original) and the proposed method (automated), from 195 processed thermal images, revealed a Mean Absolute Percentage Error (MAPE) of 11.48% in the delta temperature, which is used in the analysis of the lightning rod degradation. This result demonstrates that the method proposed in this study is feasible and allows to automate the inspection of lightning arresters. Future investigations consist of refining the segmentation process by fine-tuning hyperparameters and by using the cross-validation technique.

Key words: lightning arresters; degradation diagnosis; thermal images; deep learning; temperature extraction.

LISTA DE ILUSTRAÇÕES

LISTA DE TABELAS

LISTA DE ABREVIATURAS E SIGLAS

AI	Artificial Intelligence
AP	Average Precision
APs	Average Precision for small object
APm	Average Precision for medium object
APl	Average Precision for large object
AVG	Average
BBOX	Bounding Box Detection
CCFF	Central Contour Filtering Function
DL	Deep Learning
IoU	Intersection over Union
IoT	Internet of Things
MA	Main Axis
CNN	Convolutional Neural Network
ROI	Region of Interest
R-CNN	Region based Convolutional Neural Networks
RPN	Region Proposal Network
SDK	Software Development Kit
COCO	Common Object in Context
GIMP	GNU Image Manipulation Program
FAIR	Facebook AI Research
MAE	Mean Absolute Error
RMSE	Root Mean Squared Error
MAPE	Mean Absolute Percentage Error
℃	Celsius Degree

SUMÁRIO

1 INTRODUCTION

Lightning arresters are a vital piece of equipment in electrical systems, contributing to their reliability, economy, and safety. They are typically installed near the primary substation equipment, helping to ensure that overvoltage does not exceed the intended design specifications (FRONTIN, 2013).

Over time, lightning arresters may suffer from degradation due to several factors, such as contamination from humidity, dirt and/or rust, which can compromise their insulating capability. Other issues that may arise can be attributed to mechanical problems, such as broken shunting resistors or incorrect assembly of components (GILL, 2009). In this context, thermal inspection is an important and widely used method for qualitative and quantitative evaluation of the lifetime and degradation of lightning arresters (SILVEIRA, 2009), (COSTA et al., 2019; SANTOS, 2017).

At electrical substations, collection campaigns are conducted with the purpose of obtaining thermal images of operational high voltage lightning arresters. Once these images are obtained, they are imported into a software tool for analysis. This tool allows for the manual selection of desired sections within the arresters, and subsequently extracts the necessary temperature values from those regions (SANTOS, 2017).

The manual temperature data extraction from lightning arresters can be laborious and time-consuming, demanding human expertise which cannot be readily available or scalable. Moreover, it is susceptible to errors, which could result in inaccurate assessments of the arresters, potentially leading to severe consequences (SANTOS, 2017). This has led to a demand for more reliable and faster alternative methods. Previous studies (COSTA et al., 2019) have introduced image processing modules capable of segmenting and automatically interpreting variables from lightning arresters. However, the literature does not provide detailed information on how thermal images are processed.

Artificial Intelligence (AI), particularly its branch based on deep learning (DL) algorithms (RUSSELL; NORVIG, 2016), has become increasingly popular recently due to its demonstrated superiority over previous state of the art techniques in multiple tasks, as well as the large variety of data from various sources such as visuals, sound, medical, social, and sensor information (MACIEL et al., 2021; VOULODIMOS et al., 2018). One domain where DL has been particularly influential is computer vision (SZELISKI, 2022; VOULODIMOS et al., 2018). The ability of DL algorithms to extract and learn from complex patterns in visual data has revolutionized this field, leading to breakthroughs in tasks such

as image recognition, segmentation (HAFIZ; BHAT, 2020), and object detection (ZOU et al., 2023).

In this context, the main goal of this study is to design, test, and confirm the effectiveness of a novel method. This method, which utilizes an artificial intelligence algorithm specifically built on deep learning techniques (RUSSELL; NORVIG, 2016), aims to automate the process of extracting temperature data from lightning arresters identified in thermal images. The motivation behind this is to enhance the reliability and efficiency of lightning arrester degradation analysis. To accomplish this main goal, a set of specific objectives were outlined:

1) A review on the theoretical foundations of the lightning arresters' degradation problem;
2) Analysis of existing Artificial Intelligence tools and technologies that can be used to address the lightning arrester's problem;
3) Annotate image data, create and use a new dataset of the lightning arrester's thermal images;
4) Design and develop a Deep Learning method to extract the temperature data from thermal images;
5) Perform an accuracy evaluation test for the proposed method.

This study presents in section II the fundamentals on lightning arresters' degradation and a review related to the subject. Section III presents the proposed method. Section IV presents the results and discussion. Finally, section V displays the contributions, and future fulfillments of this study.

2 BACKGROUND AND PREVIOUS WORKS

This section describes the fundamental concepts regarding AI with DL methods for object detection. In addition, it explores recent advancements in the field of lightning arrester inspection techniques.

2.1 OBJECT DETECTION AND ARTIFICIAL INTELLIGENCE

Computer vision is a multidisciplinary field that focuses on enabling machines to interpret and understand visual information from the world around them (SZELISKI, 2022). The field of computer vision has experienced tremendous growth in recent years, primarily due to the proliferation of image data. This explosion of visual information can be attributed to the increasing number of sensors and cameras embedded in various devices, from smartphones and wearable gadgets to drones and internet of things (IoT) devices (SHAFIQ et al., 2022). According to a report by Grand View Research, the global computer vision market size was valued at USD 11.22 billion in 2021 and is expected to expand at a compound annual growth rate (CAGR) of 7.0% from 2022 to 2030 (GVR, 2023). This highlights the central role of visual data in the digital era.

As a rapidly evolving area of artificial intelligence, computer vision has found applications in numerous domains, including self-driving cars (WAYMO, 2023), robotics (CORKE, 2011), medical imaging (LITJENS et al., 2017), and security surveillance systems (HU et al., 2004), among others. These applications rely on the ability of computer vision algorithms to process and analyze images or videos, allowing machines to make informed decisions or perform specific tasks.

The overarching goal of computer vision is to emulate human vision capabilities in machines, enabling them to extract meaningful information from visual data (SZELISKI, 2022). This encompasses a wide range of tasks, such as identifying objects (KIRILLOV et al., 2023), recognizing faces (TAIGMAN et al., 2014), tracking moving objects (COIFMAN et al., 1998), and understanding scenes (GEBRU et al., 2017). By achieving these objectives, computer vision systems can not only automate various tasks that traditionally relied on human vision but also offer new possibilities for enhancing human capabilities and improving the overall quality of life (ANKRUM, 2020).

One of the fundamental techniques that make this possible is image

segmentation, a crucial process in computer vision. Image segmentation involves breaking down a digital image into multiple segments or regions, each representing a distinct object or component of the image (KANNAN; NALINI, 2014). Instance segmentation assigns unique labels to individual instances of objects within the same object-class, whereas semantic segmentation assigns a single label to all pixels belonging to the same object class in an image, this is shown in **Figure 1** (HAFIZ; BHAT, 2020). Segmentation finds applications in a wide range of fields, including object recognition, medical imaging (KAYALIBAY; JENSEN; VAN DER SMAGT, 2017), image editing, augmented reality (ABU ALHAIJA et al., 2017).

Figure 1 - Semantic segmentation (left) and instance segmentation (right).

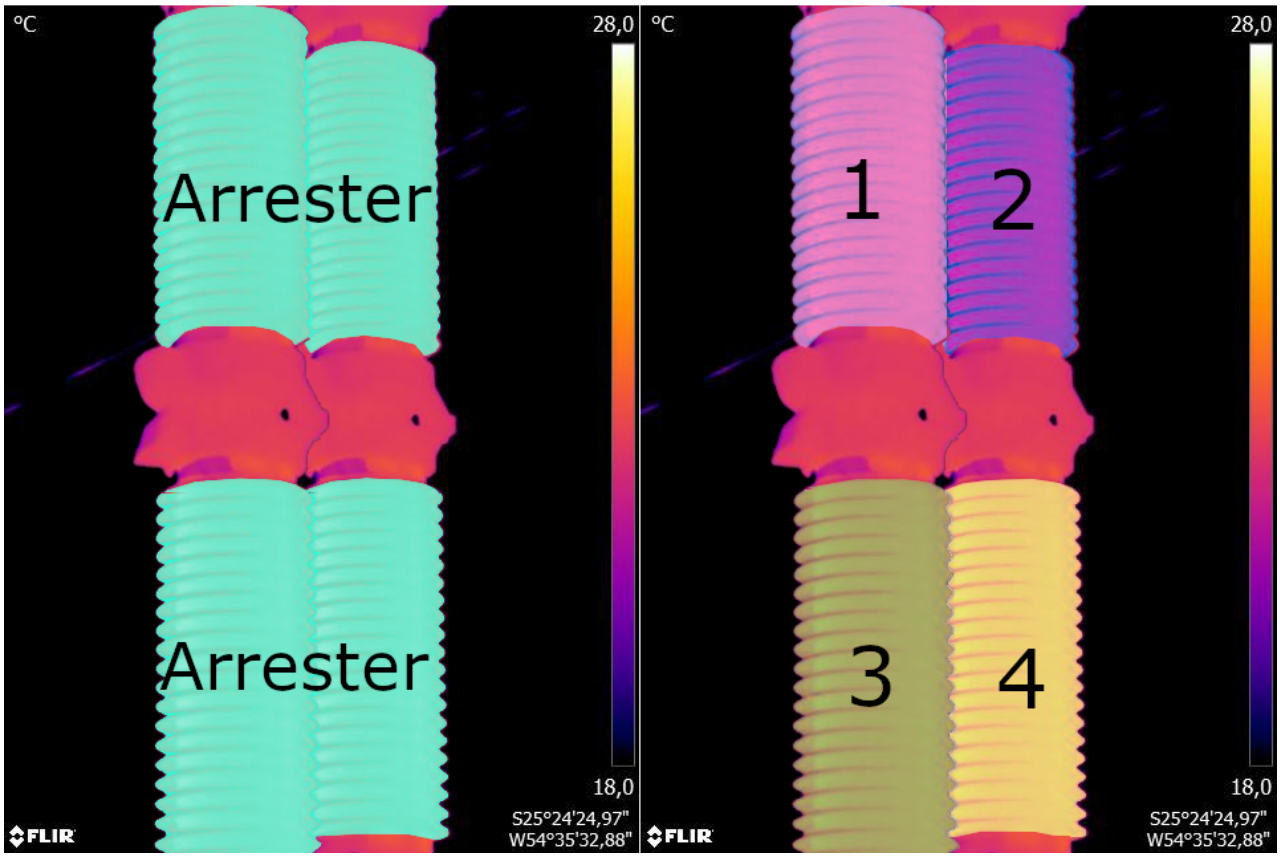

Source: The author, 2023.

In recent years, DL algorithms (LECUN; BENGIO; HINTON, 2015) such as convolutional neural networks (CNNs) have emerged as a popular approach for computer vision tasks, outperforming traditional methods in terms of accuracy and robustness. They perform better at handling geometric transformations and variations in lighting and contrast, which can often pose challenges for classic methods (OFIR; NEBEL, 2021), (SCHMIDHUBER, 2014), (ZOU et al., 2023).

The CNNs are specialized DL architectures for image analysis and computer vision tasks. they represent an advancement over traditional artificial neural networks (YEGNANARAYANA, 2009), as they are capable of effectively learning hierarchical spatial features. This ability allows them to perform tasks such as classification, localization, and segmentation with greater accuracy (KRIZHEVSKY; SUTSKEVER; HINTON, 2017). A typical CNN consists of interconnected layers, including convolutional layers, which apply filters to detect diverse features. Activation functions, like ReLU (FRED AGARAP, 2018), introduce non-linearity, while pooling layers reduce spatial dimensions and computational complexity (SCHERER; MÜLLER; BEHNKE, 2010). Fully connected layers perform high-level reasoning, and the output layer generates final predictions or classifications (ALBAWI; MOHAMMED; AL-ZAWI, 2017) a typical CNN is demonstrated in **Figure 2**.

Figure 2 - The pipeline of a typical convolutional neural network.

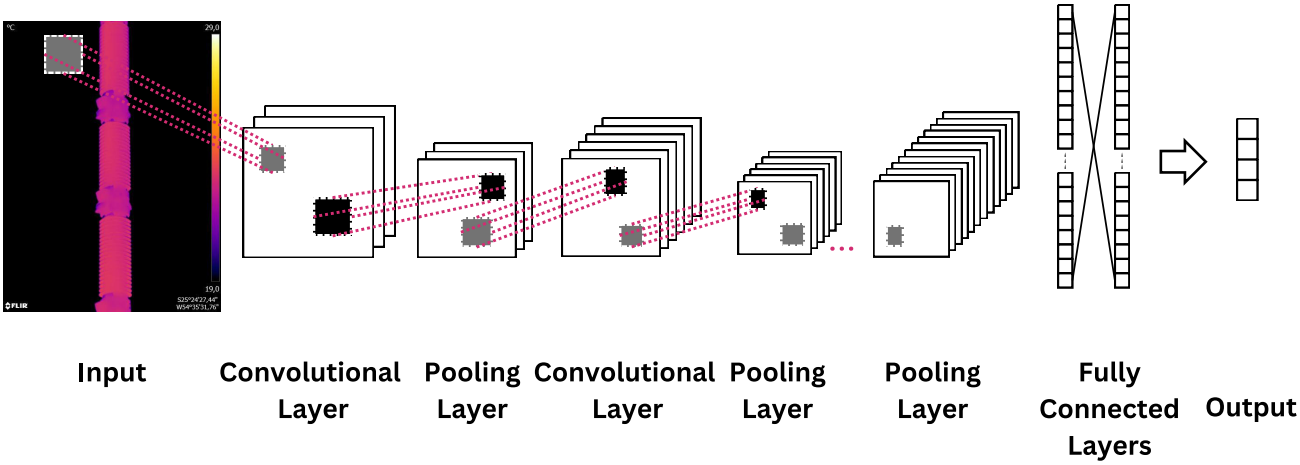

Source: adapted from (FAHIM, 2020).

However, computer vision tasks are not limited to classification problems. More complex tasks, such as object detection and segmentation, require additional processing steps and techniques. To tackle these challenges, object detection and segmentation techniques often follow a two-stage framework. In the first stage, the model generates regions of interest (ROIs) within the image, which are candidate locations that potentially contain objects. In the second stage, the model classifies these ROIs into different object classes and refines their bounding boxes for more accurate localization.

One of the early examples of a two-stage object detector is the Region-based Convolutional Neural Networks model (R-CNN) (GIRSHICK et al., 2013) . R-CNN generates ROIs using a separate region proposal algorithm, such as Selective Search

(UIJLINGS et al., 2013), Once these ROIs are determined, they undergo a warping step to standardize the sizes of the regions. Subsequently, each ROI is individually processed through a CNN to classify the object and refine its bounding box as shown in **Figure 3**.

Figure 3 – Region Convolutional Neural Network (RCNN) workflow.

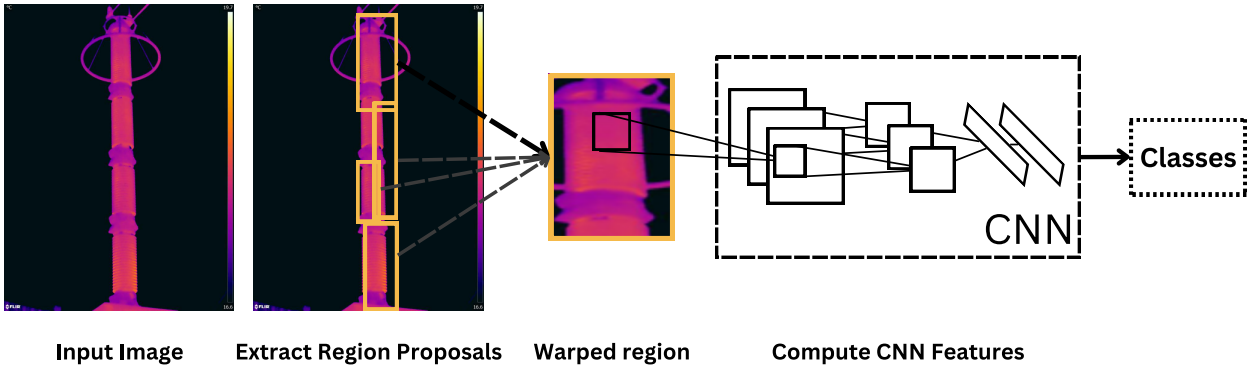

Source: adapted from (GIRSHICK et al., 2013).

R-CNN suffered from computational inefficiency due to the need to process each ROI independently. To address this issue, the Fast R-CNN significantly improves upon the previous R-CNN model by introducing novel techniques that increase computational efficiency and detection accuracy. Unlike R-CNN, which independently computes features for each proposed region, Fast R-CNN applies a convolutional neural network (CNN) to the entire image once as shown in **Figure 4**, generating a comprehensive feature map. Region proposals are then mapped onto this feature map, with each proposed region undergoing a ROI pooling operation to transform the extracted features into a fixed size suitable for fully connected layers. This process not only reduces redundancy but also accelerates both training and testing phases, as the feature extraction step is shared across all proposals. Despite these improvements, the Fast R-CNN model still relied on an external region proposal algorithm, which limited its overall efficiency and performance.

Figure 4 - Fast-RCNN workflow.

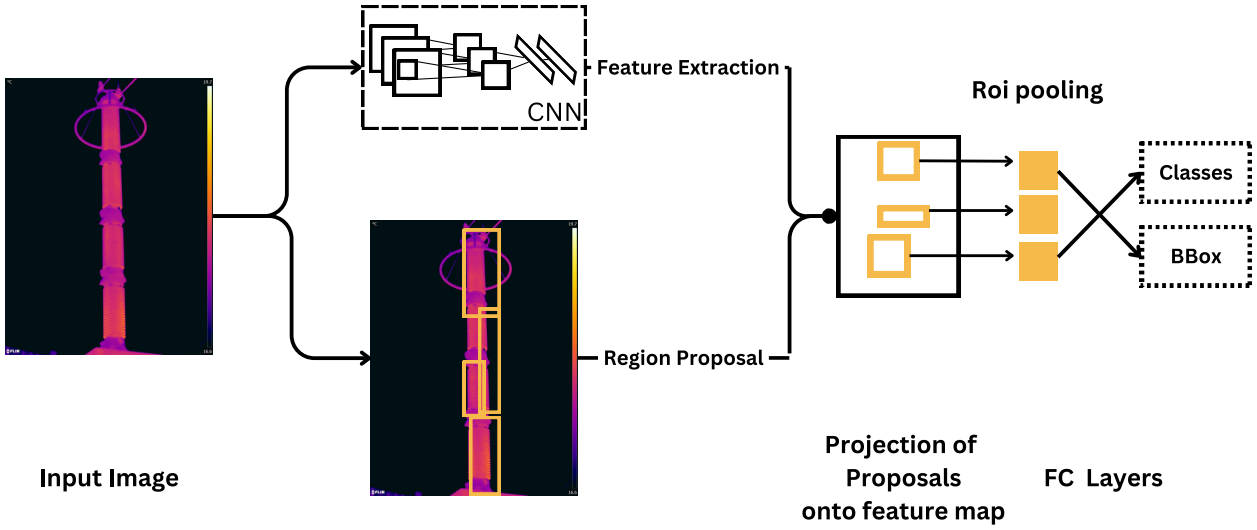

Source: adapted from (GIRSHICK, 2015).

Faster R-CNN (REN et al., 2015) builds upon the success of Fast R-CNN by introducing the Region Proposal Network (RPN), which significantly improves the speed and efficiency of object detection. While Fast R-CNN relies on selective search to generate region proposals, which is a slow and time-consuming process, Faster R-CNN incorporates a neural network-based approach for region proposal generation. This integrated approach enables Faster R-CNN to perform object detection and bounding box regression in near real-time, offering a substantial performance boost.

Mask R-CNN (HE et al., 2017) further extends the capabilities of Faster R-CNN by incorporating a parallel branch for pixel-level instance segmentation. This added component allows Mask R-CNN to not only detect objects and their bounding boxes but also generate high-quality binary masks for each object instance, providing detailed semantic information about the detected objects. To enhance the accuracy of mask predictions, Mask R-CNN introduces RoIAlign, a more precise method for extracting RoI features that eliminates quantization errors caused by RoIPool in Faster R-CNN (BHARATI; PRAMANIK, 2020). The Mask R-CNN architecture consists of three main components: the backbone network, the RPN, and the parallel heads for classification, bounding box regression, and mask prediction. These components work together to efficiently detect objects, classify them, and generate accurate instance segmentations (BHARATI; PRAMANIK, 2020; HE et al., 2017).

i. **Backbone Network**: The backbone network is a deep CNN responsible for extracting features from the input image. These features are used by the

subsequent components of the Mask R-CNN architecture to generate ROIs, classify objects, and predict bounding boxes and masks. Common backbone architectures, such as ResNet (HE et al., 2015) and VGG (SIMONYAN; ZISSERMAN, 2014), are often used in Mask R-CNN.

ii. **Region Proposal Network (RPN):** The RPN is a crucial part of the Mask R-CNN architecture that generates regions of interest (ROIs) by proposing potential object locations in the image. The RPN shares its convolutional layers with the backbone network, which allows it to generate proposals by leveraging the features extracted by the backbone.

iii. **Parallel Heads:** The parallel heads in Mask R-CNN are responsible for classification, bounding box regression, and mask prediction. These heads operate on the ROIs generated by the RPN and share the same feature maps, allowing them to perform their tasks in parallel. The classification head determines the object class, the bounding box regression head refines the coordinates of the bounding boxes, and the mask prediction head generates binary masks, for instance segmentation, through pixel-wise classification. According to (HE et al., 2017; YAHUI PENG et al., 2019), the complete Mask R-CNN architecture is demonstrated in **Figure 5.**

Figure 5 - The architecture of Mask R-CNN.

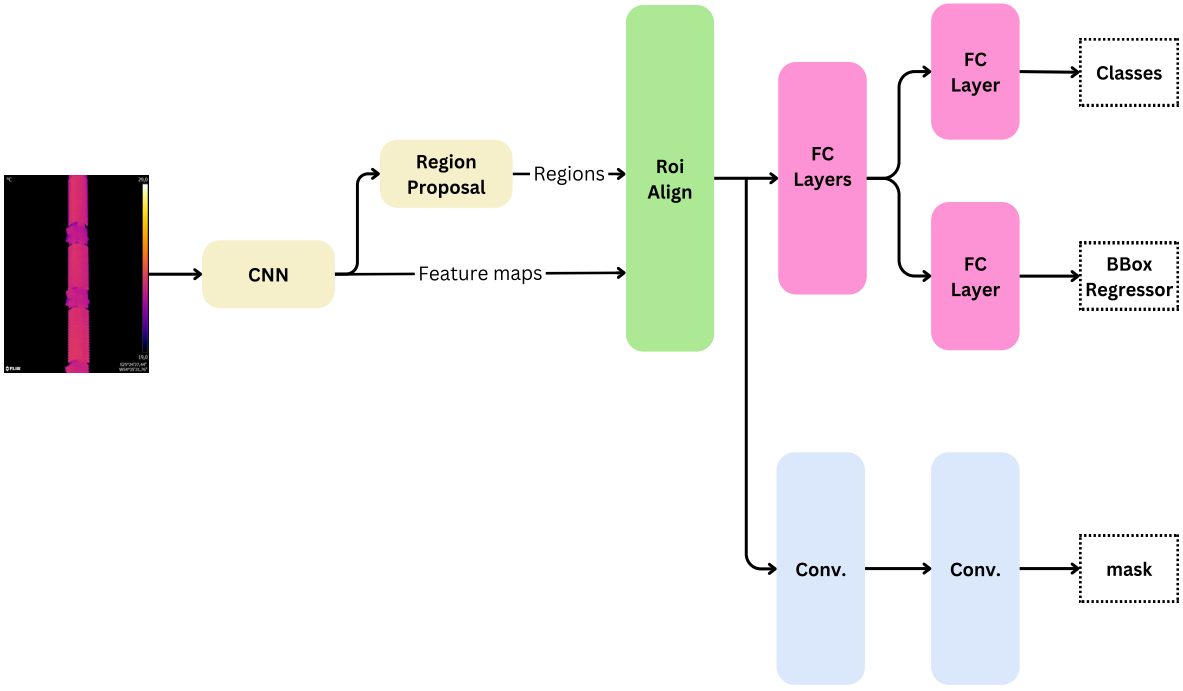

Source: Adapted from (YAHUI PENG et al., 2019).

In **Figure 5** first a CNN extracts features from the input image. These features are then processed by an RPN to generate ROIs. The ROI Align layer corrects misalignments between the RoIs and the feature map, producing fixed-size outputs for each proposal. Finally, the aligned RoIs are passed through three parallel heads: classification, bounding box regression, and mask prediction. This process results in the detection, classification, and segmentation of objects within the image.

In our work, we adopted the Mask R-CNN framework to localize and segment lightning arresters in images due to its superb ability to realize both object detection and instance segmentation tasks, and due to its popularity in similar works (ATTARD et al., 2019; KUMAR; KUKREJA, 2022; NAFI'I; YUNIARNO; AFFANDI, 2019; POLAT et al., 2020; ZHANG; CHANG; BIAN, 2020).

2.2 LIGHTNING ARRESTERS DEGRADATION

To enhance diagnostic and evaluation capabilities, numerous technical-scientific and technological studies have been conducted. Huang et al (HUANG; HSIEH, 2014) proposed an approach for improving the predictive maintenance of Zinc Oxide (ZnO) lightning arresters through online resistive leakage current monitoring and infrared image inspection, using a regression model-based fault diagnosis. This method aims to provide better diagnostic results compared to traditional methods and to reduce reliance on engineers' experience by incorporating statistical analysis (HUANG; HSIEH, 2014).

On the other hand, Laurentys et al. presents the DIPRA system, a computational tool developed by Center for Energy Research CEPEL (CEPEL, 2023), designed to assess the operational condition of ZnO and Silicon Carbide lightning arresters. The system leverages a combination of techniques, including infrared thermography, radio interference, and leakage current monitoring, to generate both partial and comprehensive diagnoses. The DIPRA system comprises several modules that collaboratively work to ensure precise diagnoses. The output data from these modules are processed using artificial neural networks. Subsequently, the lightning arrester's condition is classified into one of four categories: mild, normal, suspicious, or defective.

The article states the inclusion of a digital processing module for thermograms in the DIPRA system, which enables segmentation and automated interpretation of variables from the lightning arresters. However, it does not elaborate on the

specific methods employed in the processing of thermal images.

More recently, SANTOS (2017) presented an innovative diagnostic method for high-voltage ZnO lightning arresters using the Two-Valued Paraconsistent Annotated Logic (LPA2v), which is a is a logical framework used for handling contradictory and incomplete information in decision-making processes (SILVA FILHO, 2006). By analyzing temperature measurements, obtained through infrared thermography and data from the third harmonic component of the resistive leakage current, the study aims to provide a more accurate assessment of the arresters' condition. The author conducted two collection campaigns covering ZnO arresters installed in various voltage systems and statistically analyzed the data to obtain mean and standard deviation values. These values were then used as input variables for the LPA2v, which presents the results as a graph, indicating the current condition of each arrester. The proposed method demonstrates the potential of LPA2v in assisting utilities with decision-making, regarding the optimal time for replacing equipment, ultimately enhancing the reliability and safety of electrical installations (SILVA FILHO, 2006) . For this method, temperature data of the Main Axis (MA) of each segment of arresters were extracted manually as shown in **Figure 6**. The maximum and average temperature were extracted, and their difference (delta) was calculated. The extraction of the temperature was done manually using Flir Tools (TELEDYNE, 2023a) which is an image processing tool which extracts the temperature values.

Considering the existing literature studies the need to develop an automated method for the measurement and extraction of temperatures from lightning arresters, this study proposes the creation of a new thermal image synthetic dataset in conjunction with the development of a novel automatic method to make temperature extraction with DL (RUSSELL; NORVIG, 2016) from thermal images. The new proposed approach automatically detects the lightning arrester (segmentation) and captures its temperature in the desired area, namely the MA. Furthermore, the methodology and respective source code for the new synthetic dataset, including the experimental analysis, will be made available to facilitate the advancement of future research. Therefore, the next section presents the methodology design, tools and technologies employed in this study.

Figure 6 - Software used to extract arresters' temperatures from the main-axis.

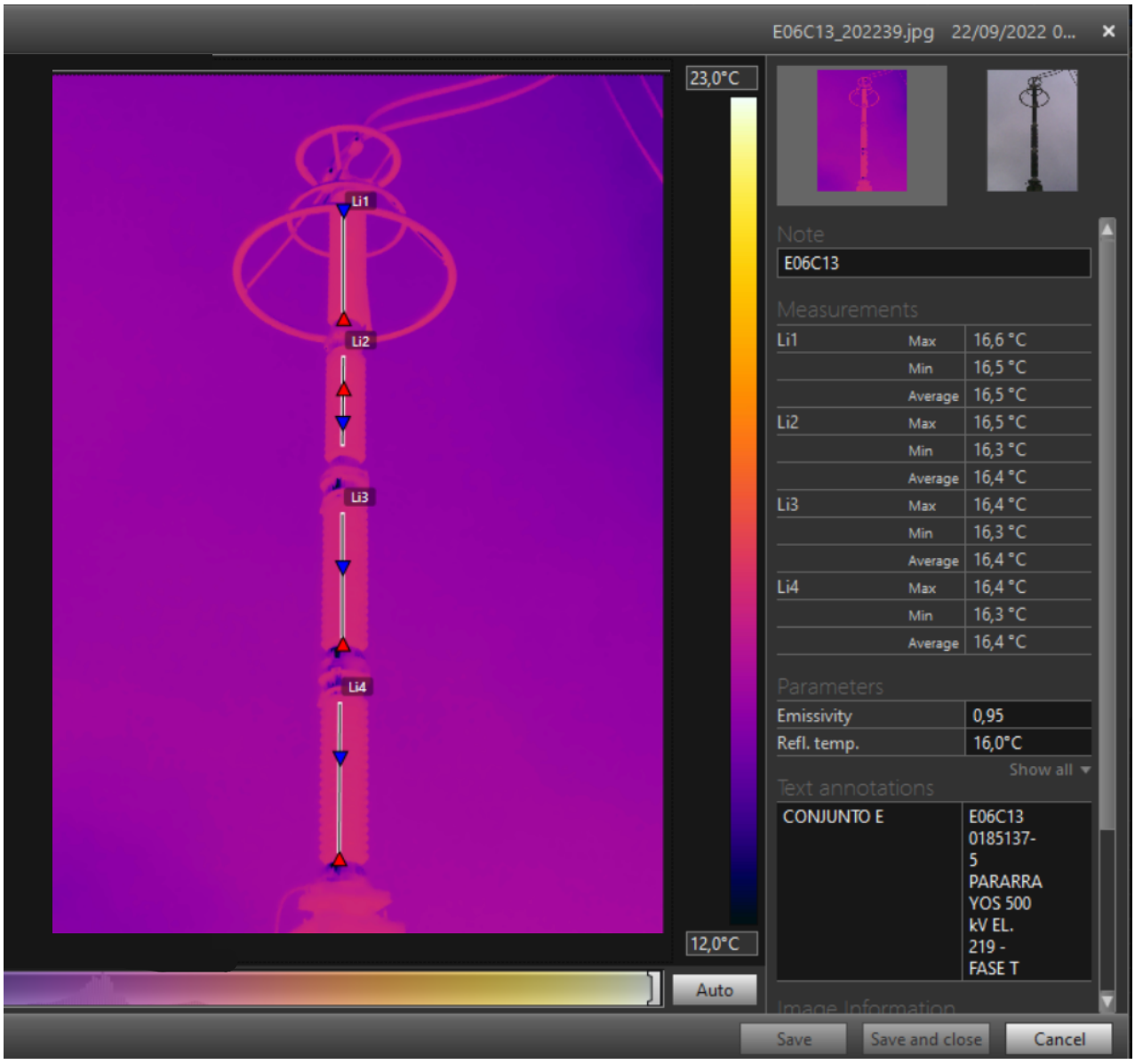

Source: The author, 2023

3 MATERIALS AND METHOD

In this section, we provide a comprehensive overview of the method proposed in our study, which encompasses the creation, annotation, and augmentation of the dataset, followed by the training of a DL model for the detection of arresters. Subsequently, the method focuses on the extraction of key data from the identified areas of interest, specifically the main axes of the arresters, using the software development kit (SDK) provided by the thermal camera manufacturer (TELEDYNE, 2023b). Finally, the design of the experimental evaluation of the proposed method is presented.

The schematic representation of the entire methodology is presented in **Figure 7**, which offers a visual guide to the various stages involved in this process. As depicted, the methodology involves creating a dataset by annotating existing thermal images, followed by augmenting the dataset and splitting it for training purposes.

Figure 7 - A general schematic representation of the proposed method.

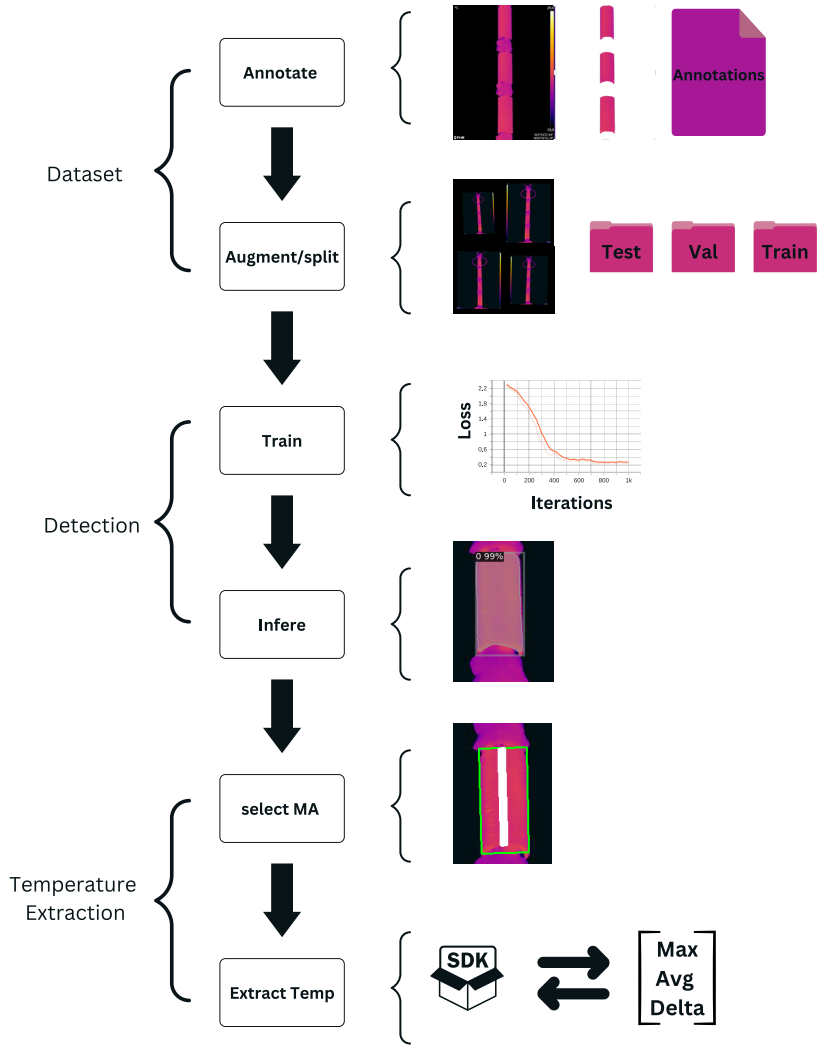

Source: The author, (2023).

As displayed in **Figure 7**, after training, the model is employed to detect arresters during the inference phase. Subsequently, the Main Axis (MA) of each section is chosen for temperature extraction using the SDK. A more comprehensive and detailed explanation of the method will be presented in the following subsections.

3.1 DATASET DESCRIPTION

The primary aim of this dataset is to facilitate the training and testing of a Mask R-CNN model, for instance segmentation of lightning arresters. To this end, we compiled a dataset consisting of 198 high-resolution thermal images (480 x 640 pixels), as illustrated in **Figure 8**. These images were captured using a FLIR T660 camera (TELEDYNE, 2023c). Following image acquisition, the dataset was annotated in the Common Object in Context (COCO) format. Recognizing the limited number of images, we implemented synthetic augmentation, increasing the dataset by a factor of 90. This augmentation process aimed to generate a more robust and diverse dataset, enabling a comprehensive investigation of the performance and characteristics of lightning arresters under various conditions.

Figure 8 - Four samples of the original dataset containing different arresters.

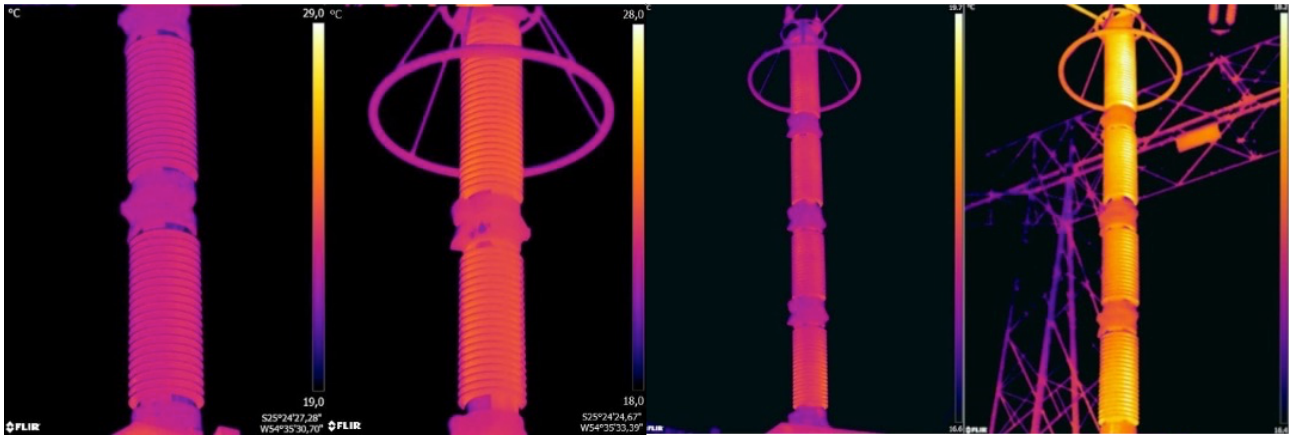

Source: Adapted from (SANTOS, 2017).

3.1.1 Image Annotation

Annotation is the process of labeling elements within an image or a dataset to provide context and information for machine learning models. In this study, the GNU Image Manipulation Program (GIMP) (KIMBALL et al., 2010) was utilized for the annotation

process. GIMP is a powerful, open-source, and free image editing software, chosen for its advanced selection tools that facilitate the manual annotation process.

In this work we employed a publicly available Python script, primarily utilizing the OpenCV library (BRADSKI, 2000), which was written to identify the contours, masks, and areas of the objects within the *.PNG images and store them. An example is shown in **Figure 9**. Where from the original image (left) the arrester sections were selected using the selection tools and stored.

Figure 9 - Original image (left) and selected sections of the arrester (right).

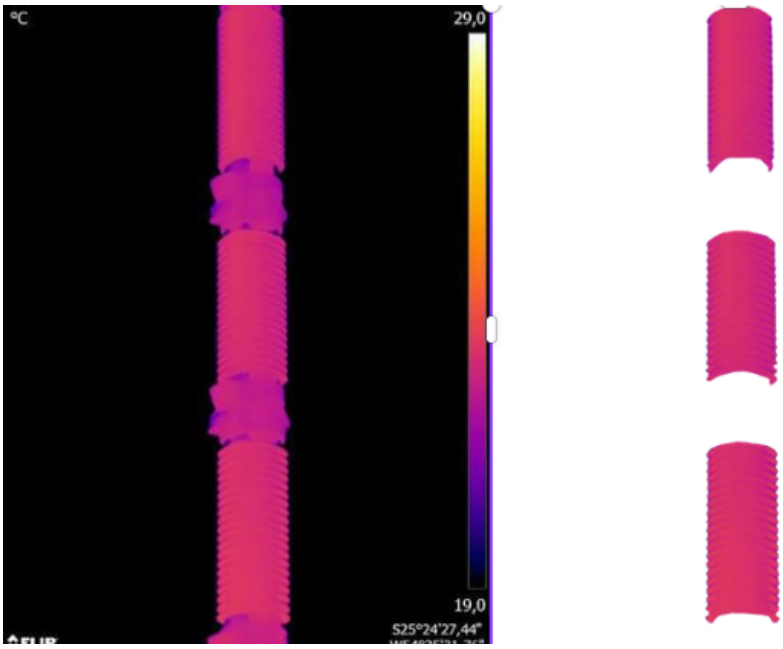

Source: Adapted from (SANTOS, 2017).

Subsequently, a second Python script was utilized to store the extracted contour information in an annotation file. This annotation file adhered to the structural specifications of the COCO format (LIN et al., 2014). These scripts are available upon request to the author.

3.1.2 Splitting and Augmentation

This subsection covers the methodology employed for the splitting and augmentation of the dataset. Dataset splitting is an essential practice in DL paradigms aimed at mitigating the risk of model overfitting, thereby enhancing its ability to generalize effectively to unseen data (PEREZ; WANG, 2017). This process typically entails partitioning the dataset into distinct subsets: i) the training set for model building, ii) the validation set for

future hyperparameter optimization and model selection and, iii) the test set for an unbiased evaluation of the finalized model.

The dataset was divided, with 10% of the images allocated for testing. This division of data into separate training and testing sets prevents overfitting and ensures that the model generalizes well to new, unseen data.

Following the data split, the training images were augmented using the Imgaug library (JUNG et al., 2020), which performs various transformations on images and their corresponding annotations. The dataset was artificially expanded by applying transformations to the original images, such as rotation, flipping, and changes in brightness. An example of these transformations applied to one image are shown in **Figure 10**.

Figure 10 – Augmented sample images from one original arrester image.

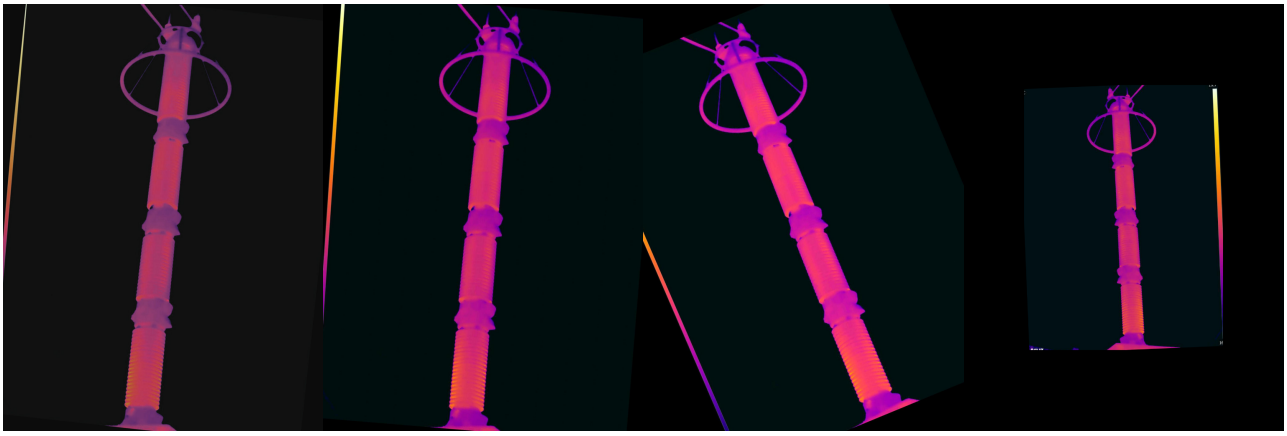

Source: Adapted from (SANTOS, 2017).

In this study, each image in the training set was augmented by applying a series of transformations, effectively increasing the dataset size by a factor of 90. After the augmentation process, the training data was further divided into an 80/10/10 split for training and validation and testing purposes, respectively. This additional separation is crucial for evaluating the performance of the model during the training process. A flowchart of the entire splitting and augmentation process is demonstrated in **Figure 11**.

Figure 11 - Flowchart of the splitting and augmentation process.

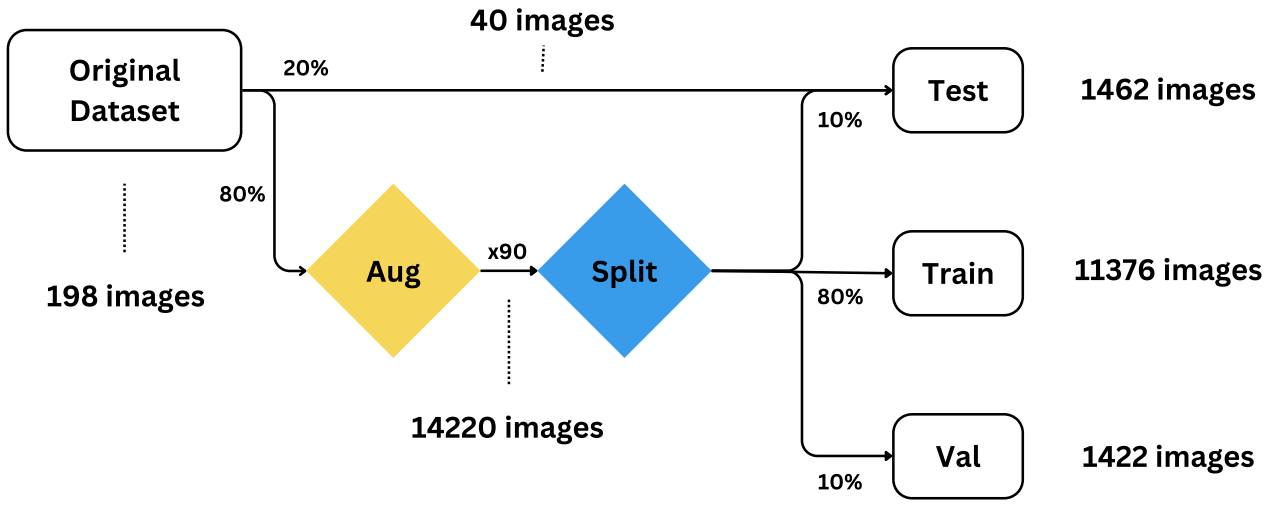

Source: The author, (2023).

3.2 AUTOMATIC TEMPERATURE EXTRACTION METHOD

This subsection describes the proposed method for automatically extracting temperature from thermal images of lightning arresters. The process begins with the detection of the arresters using the DL algorithm based in Mask R-CNN (HE et al., 2017), followed by temperature extraction from the regions of interest within the arrester using OpenCV library.

3.2.1 Lightning Arrester's Detection

As mentioned, for the detection the lightning arresters by segmentation, a Mask-RCNN was used, namely the implementation of an open-source object detection and segmentation platform developed by Facebook AI Research (FAIR) named Detectron2 (WU et al., 2019a).

The training (RUSSELL; NORVIG, 2016) process was conducted on Google Colab (BISONG, 2019), a cloud-based research platform that offers free access to computing resources, including Graphical Process Units (GPUs). In this instance, Transfer Learning technique (WEISS; KHOSHGOFTAAR; WANG, 2016) is employed to adapt a pre-trained Mask R-CNN model (WU et al., 2019b) with a ResNet-50 backbone and Feature Pyramid Network (FPN) for a new segmentation task. The model, which was initially trained on the COCO dataset, is fine-tuned on our custom dataset tailored for this specific problem

involving only the arrester class. Various hyperparameters, such as learning rate, batch size, and maximum number of iterations, are adjusted to suit the requirements of this problem. The hyperparameters were set according to **Table 1**.

Table 1 - The hyperparameters used in training the Mask-RCNN model for lightning arresters' segmentation and detection.

Hyperparameter	Value
Images per Batch (IMS_PER_BATCH)	4
Base Learning Rate (BASE_LR)	0.00025
Maximum Iterations (MAX_ITER)	4000
Learning Rate Decay Steps (STEPS)	1600, 3000
Decay Factor (SOLVER.GAMMA)	0.7
RoIHead Batch Size per Image (BATCH_SIZE_PER_IMAGE)	128
Number of Classes (NUM_CLASSES)	1

Source: the author, 2023.

The training process lasted 1 hour and 10 minutes; the associated total loss and Mask-RCNN accuracy to iterations profile is demonstrated in **Figure 12**. Where iterations refer to the number of times the model updates its weights during training and total loss is a scalar that quantifies how well is the model performing in the tasks of object classification, bounding box regression, and mask prediction.

Figure 12 - Total loss (left) and accuracy (right) of the used Mask - RCNN model.

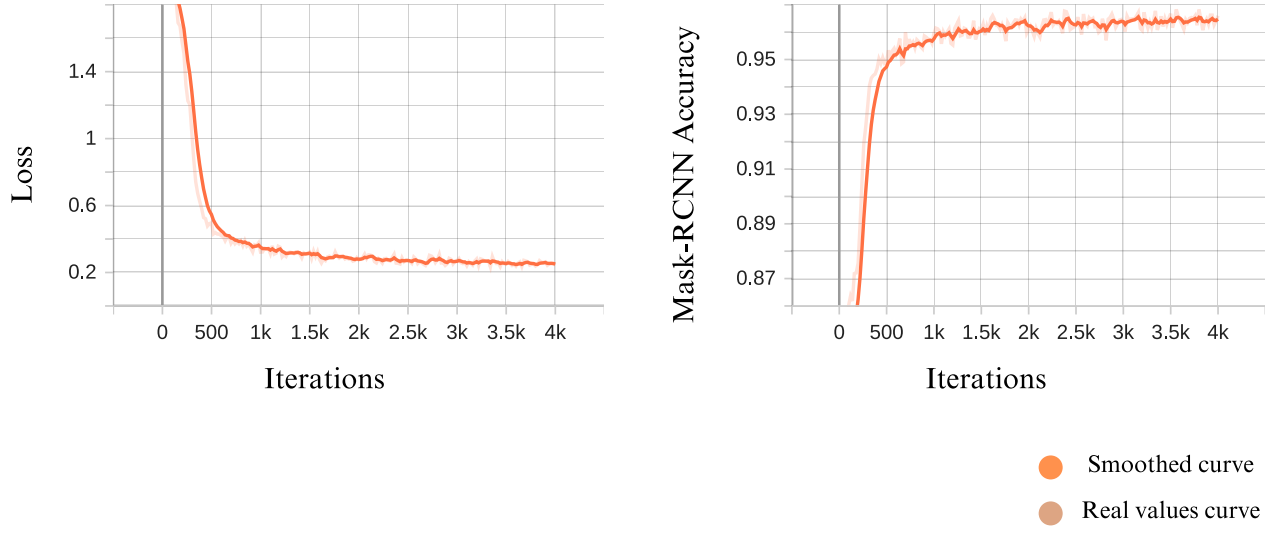

Source: The author, 2023.

As can see in **Figure 12**, the model learns quickly in the early iterations and reaches a limit where the loss and accuracy do not change significantly. The performance of the model will be discussed in the results section in more detail. The **Figure 13** demonstrates how the trained model can identify arresters within test images not previously encountered during the training process. This outcome highlights the model's ability to

generalize effectively to new instances, showcasing its potential for practical application in real-world scenarios.

Figure 13 – Lightning arresters inference by the trained model on a test image.

Source: The author, (2023).

To address the challenges presented by complex images, such as those depicted in **Figure 14,** where multiple arresters are present or components resembling arresters are in proximity, an essential aspect has been taken into consideration. Specifically, the arrester of interest is consistently positioned at the center of the image. Consequently, an additional function was implemented namely Central Contour Filtering Function (CCFF) to exclusively select the central contours of the image, thereby enhancing the accuracy and reliability of arrester identification and analysis.

Figure 14 - Comparison of contour selection before (left) and after (right) applying the proposed Central Contour Filtering Function (CCFF).

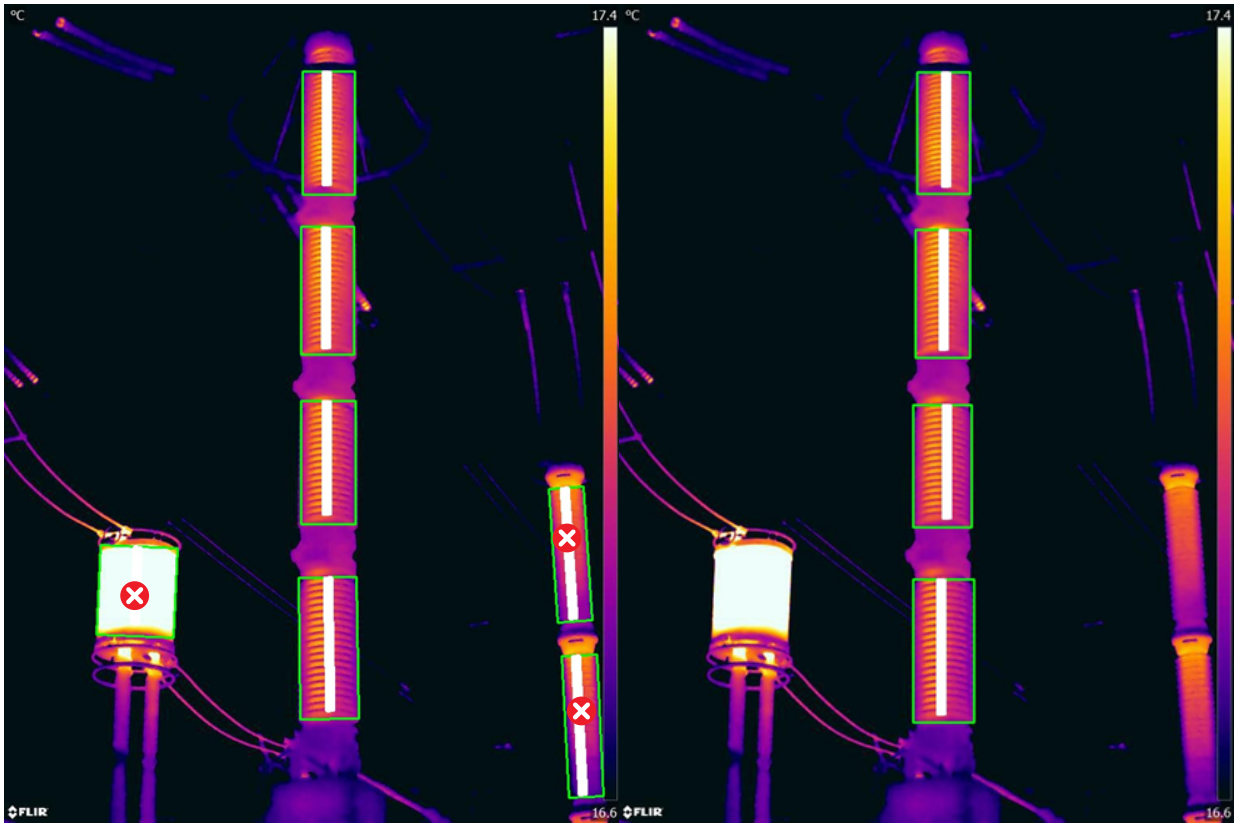

Source: The author, 2023.

As demonstrated in **Figure 14,** the CCFF function operates by calculating the center of mass for each contour and the distance of each contour center to the middle of the image along the x-axis. It then identifies the contour closest to the center along the x-axis and filters contours whose x-coordinate is within a specified tolerance from the closest contour, effectively focusing on the contours located near the center of the image.

3.2.2 Temperature Extraction from Lightning Arresters

A model has been developed to accurately identify lightning arresters within images. The subsequent phase entails extracting temperature data for specific components of the arrester, particularly the MA. To accomplish this, the FLIR Tools SDK is utilized. The SDK processes a thermal image as input and generates a two-dimensional matrix representing the temperature values of individual pixels as demonstrated in **Figure 15**. Nevertheless, this study requires temperature data acquisition solely for distinct regions of the lightning arresters.

Figure 15 - Input image (left) and output matrix (right) of the Flir tools SDK.

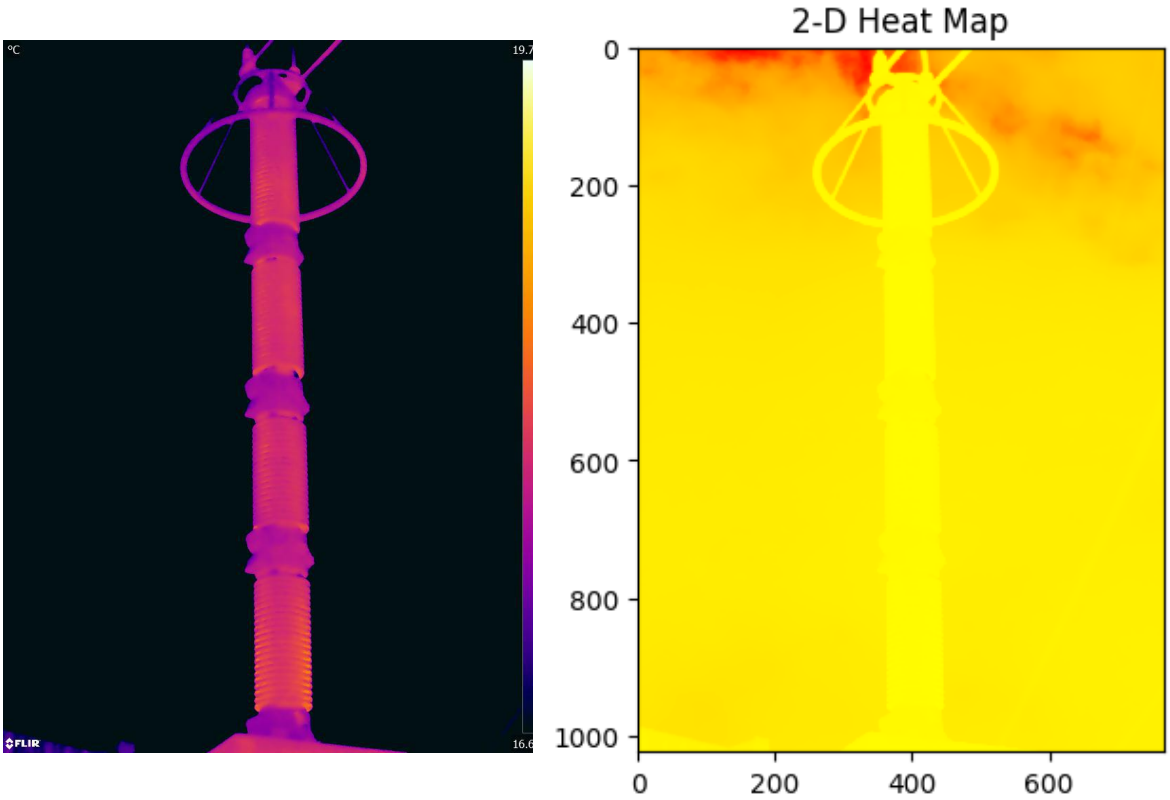

Source: The author, 2023.

To address this requirement, a custom script has been devised to selectively extract the desired pixels. This approach capitalizes on the masks produced by the Mask R-CNN model to pinpoint regions of interest. In **Step 1** algorithm by computing the minimum bounding rectangle (highlighted in blue) that encloses the arrester mask, as depicted in **Figure 16** and simultaneously identifies the corresponding contours (represented in red). In **Step 2**, the algorithm calculates the major axis (indicated in black) of the rectangle. In **Step 3** it determines the intersection points between the major axis and the contours, finally in

Step 4 all the points located between these intersections (highlighted in orange) are extracted. The resulting line, with a width of one pixel, is adjusted to a variable width, resulting in the final delineation of the pixels of the MA. In the process of iterative comparison to ascertain the optimal pixel width for the MA, a 4-pixel width emerged as the most effective, and hence, was the selected choice.

Figure 16 - A visualization of the algorithm to select the interest main-axis area.

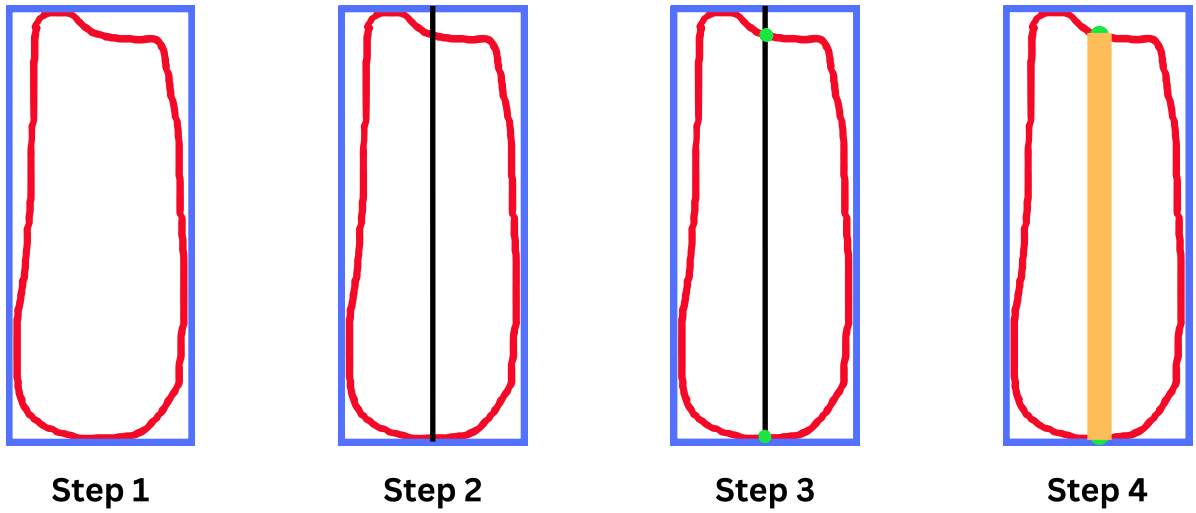

Source: The author, 2023.

For each point within the resulting area, the temperature is acquired using the matrix returned by the SDK. Subsequently, the average (avg), maximum (max), and delta temperatures of each line are computed and stored in a tuple.

3.3 EXPERIMENTAL EVALUATION DESIGN

In this section, we detail the design of our experimental evaluation for the proposed method of automatic temperature extraction from lightning arresters. For this we note that our evaluation is centered on two primary objectives:

1) Assessing the performance of the Mask R-CNN in image segmentation.

2) Determining the accuracy of our proposed method in extracting temperature data from lightning arresters.

Evaluating the performance of segmentation models necessitates the use of specific metrics, one of which is Average Precision (AP), which provides an aggregate measure of the model's precision in correctly detecting and segmenting objects within a set of images

(PADILLA; NETTO; DA SILVA, 2020).

The specificity of what we regard as a correct prediction can be adjusted using the Intersection over Union (IoU) threshold, which quantifies the degree of overlap between the predicted and actual object regions. In this study AP will be evaluated at IoU thresholds of 50% and 75%, represented as AP50 and AP75 respectively. This offers insights into the model's performance under different stringency levels.

Moreover, to ensure a comprehensive understanding of a model's capabilities, AP is evaluated for small (APs), medium (APm), and large (APl) objects. This stratification of object sizes allows us to discern potential variations in model performance, as some models may excel at detecting larger objects but struggle with smaller ones. Overall, by assessing AP across various IoU thresholds and object sizes, we gain a nuanced understanding of the model's performance in instance segmentation tasks.

To evaluate the performance of the proposed method for extracting temperatures of arresters, we compare the temperatures derived using our automatic method to those obtained manually in a previous work (SANTOS, 2017). However, it is crucial to acknowledge that the manually extracted temperatures, while treated as the ground truth in this work, may not be infallible. Operator-dependent variability introduces the possibility of inherent errors in these reference measurements (SANTOS, 2017). Therefore, while employing these manual data to evaluate the accuracy of our proposed method can offer insights into its reliability, it may not necessarily provide an exact measure of the method's true accuracy.

A dataset consisting of 203 images was acquired from SANTOS (2017)., where an operator manually processed the images using FLIR tools software to identify the MA (white line) of each arrester section as shown in **Figure 17.** This information was saved in the metadata of the images.

By utilizing the identified lines, temperatures were extracted, and the average, maximum, and delta values were computed. Consequently, a tuple of (avg, max, delta) was obtained for each image in the dataset. Subsequently, the proposed automatic method was applied to the same set of images to generate a similar tuple for each image, demonstrates how the evaluation process occurs (**Figure 18**).

Figure 17 - A manually processed image of an arrester in which the main-axis of each section was selected.

Source: (SANTOS, 2017), 2017.

Figure 18 – Comparative evaluation of the proposed method for automatic temperature extraction.

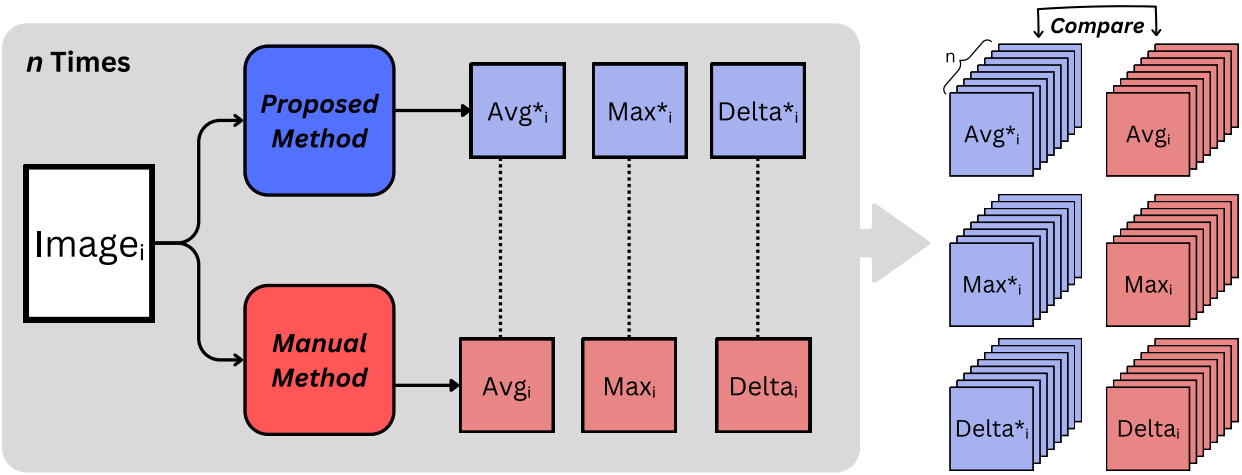

Source: the author, 2023.

As shown in **Figure 18,** each image denoted by “I” undergoes processing through both the proposed algorithmic approach and the manual method, resulting in corresponding tuples of the form (avg, max, delta). This procedure is repeated for “n” times across all the images. Following this, the “avg*” temperatures generated via the proposed method are collated and juxtaposed with those extracted via the manual method. A similar process is subsequently conducted for the “max” and “delta” components of the tuples.

In the pursuit of comprehensive analysis, it's crucial to highlight that although our primary interest lies in the delta temperature, we will extend our comparison to encompass both maximum and minimum temperature values. This broader approach will afford a more robust understanding of the areas where the method may demonstrate greater susceptibility to failure. Through this approach, we aim to capture a more complete picture of the method's performance under various conditions, thus enabling a more nuanced interpretation of its strengths and weaknesses.

To effectively compare the results, three evaluation metrics were utilized: Mean Absolute Error (MAE) expressed in **Equation (1)**, Root Mean Squared Error (RMSE) as outlined in **Equation (2)**, and Mean Absolute Percentage Error (MAPE), described in **Equation (3).** Each metric serves a distinct purpose in assessing the model's performance.

$$MAE = \frac{1}{n}\sum_{i=0}^{n}|x_i - \hat{x}_i| \quad \textbf{(1)}$$

$$RMSE = \sqrt{\frac{1}{n}\sum_{i=0}^{n}(x_i - \hat{x}_i)^2} \quad \textbf{(2)}$$

$$MAPE = \frac{1}{n}\sum_{i=1}^{n}\left|\frac{x_i - \hat{x}_i}{x_i}\right| \quad \textbf{(3)}$$

where:

- n is the number of observations;
- x_i is the manual method value of i^{th} arrester temperature (avg or max or delta);
- $\hat{x}_i$ is the proposed method value of the i^{th} arrester temperature (avg or max or delta).

The MAE (℃) measures the average magnitude of errors, providing a clear representation of prediction accuracy. The RMSE (℃) emphasizes larger errors, assessing the model's sensitivity to outliers. The MAPE (%), expressing errors as a percentage of actual values, allows for comparison across different scales or datasets.

To further assess the similarities and discrepancies between the two methods, scatter plots are generated, with each data point's x and y coordinates corresponding to the respective values from the manual and proposed methods. This visualization will facilitate the identification of outliers, thereby providing insights into the similarities of the methods.

4 RESULTS AND DISCUSSION

In this section, we will discuss two key aspects of our findings: The accuracy of detection and segmentation of the arresters (section 4.1), and the overall precision of our proposed method in automatically extracting temperature from lightning arresters.

4.1 ARRESTER'S SEGMENTATION AND DETECTION

The evaluation results from the Mask R-CNN model, employed for both Bounding Box Detection (BBOX) and Segmentation, can be represented in a tabular form, as shown in **Table 2.**

Table 2 - Performance Evaluation of Mask R-CNN for Bounding Box Detection and Segmentation.

Evaluation Component	AP	AP50	AP75	APm	APl
BBOX	85.850	98.855	97.659	77.395	88.547
Segmentation	83.850	98.855	96.579	61.817	86.650

Source: The author, 2023.

The results from the Mask R-CNN model, presented in **Table 2,** reveal high proficiency in object detection and segmentation. This is evident from the high AP50 and AP75 scores, indicating effective identification and localization of objects with moderate to high overlaps with the ground truth. The AP accounts for the IoU between 50 and 95 for large and medium objects. Small objects were intentionally excluded from this measure due to their scarcity and relative insignificance, as they represent minor portions of the arresters.

The model's performance varies with object size, as seen in the APm and APl scores. For both bounding box detection and segmentation, the model shows superior performance on large objects compared to medium-sized objects. This disparity suggests potential room for improvement in the model's performance.

It's noteworthy that while the precision is high, it doesn't necessarily mean that every boundary of the arrester is captured with the same degree of accuracy. While the model can localize an arrester, some of the peripheral boundaries might not be precisely defined. This, however, does not diminish the model's utility, because our focus is not on achieving a perfect segmentation, but localizing the MA of the arresters.

The primary advantage of this approach, and one that significantly outweighs these minor drawbacks, is the significant improvement in method speed. With the implementation

of this segmentation, our method can infer at a considerably fast rate of just 2 seconds per image.

4.2 PROPOSED METHOD ACCURACY

In this subsection, our objective is to assess the performance of the proposed method through the application of quantitative metrics and visual representations. Following the evaluation, we will conduct an in-depth analysis of the outliers and conclude by discussing the advantages and disadvantages associated with the proposed approach.

4.2.1 Experimental Evaluation

The experimental evaluation of the proposed method for automatic temperature extraction, from lightning arresters, are detailed in **Table *3***. The performance of the proposed method, compared to the actual and manual approach used in (SANTOS, 2017), is described from the three measures of accuracy (MAE, RMSE and MAPE).

Table 3 - Comparison of the automatic to the manual temperature extraction methods using statistical metrics to evaluate its performance and similarity.

Measurement	MAE (℃)	RMSE (℃)	MAPE (%)
Maximum	0.18	0.50	0.84
Average	0.06	0.13	0.43
Delta	0.17	0.46	17.58

Source: The author, 2023.

Considering the results present in **Table *3***, the following key insights and findings can be deducted:

i. The MAE showed a difference of 0.06°C for average temperature readings and 0.18°C for maximum readings. This aligns with the expectation that average readings, being mean values, are less susceptible to errors and less sensitive to extreme values than maximum readings, which are based on single pixel intensities;
ii. The slightly higher values of RMSE compared to MAE indicate that there might be occasional larger discrepancies between the two methods, as RMSE is more sensitive to larger errors;
iii. The MAPE for the differences between the temperature readings was found to be notably higher at 17.58%. This higher MAPE value can be attributed

to the fact that the difference values are close to zero;

iv. Overall, these error metrics suggest that the two methods demonstrate a high degree of similarity in their average and maximum temperature readings.

Complementary to the results depicted in **Table 3,** the comparative correlation graph of the measures between two methods (manual and proposed or automatic) can be found in **Figure 19.**

Figure 19 - Comparative analysis of temperature measurements using auto and manual methods for average, maximum, and difference values.

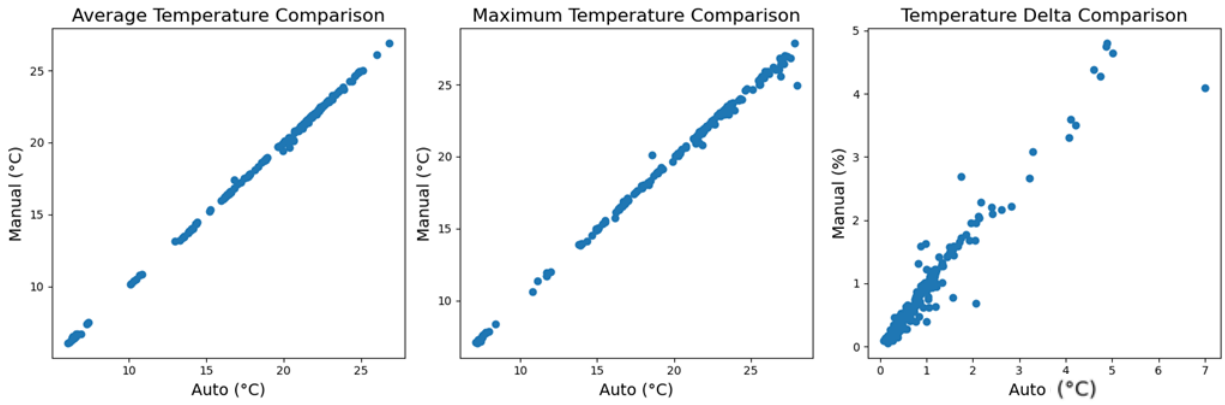

Source: the author, 2023.

As can be seen in **Figure 19,** in each of the graphs, the data points can be approximated by a line passing through the origin, thereby suggesting a certain similarity in the computation of average, maximum, and delta temperature values between the two methods. However, a few data points exhibit greater relative deviation, which are indicative of outliers. These outliers warrant further examination presented in the next subsection.

4.2.2 Outliers

Outliers are data points or observations that deviate significantly from the general trend or distribution of the dataset (RUSSELL; NORVIG, 2016). In **Figure 19**, such points are evident. To further investigate these outliers, a script was developed to extract the images corresponding to instances where the MAPE of the delta exceeds 40 percent, facilitating visual examination. The 40% threshold was selected based on the observation that it effectively encapsulated the majority of data points, allowing for the identification of those points that exhibited significantly higher error rates and therefore represented potential

anomalies in the dataset.

The first arises when the primary axes from both methods do not align. This misalignment may be attributed to incorrect segmentation by the model or potentially to operator error as shown in the examples of **Figure 20** where the thick white line is the MA of the proposed method, and the thin white line is the MA selected by the manual method.

Figure 20 - First type of error – Main-Axis misalignment between the two methods.

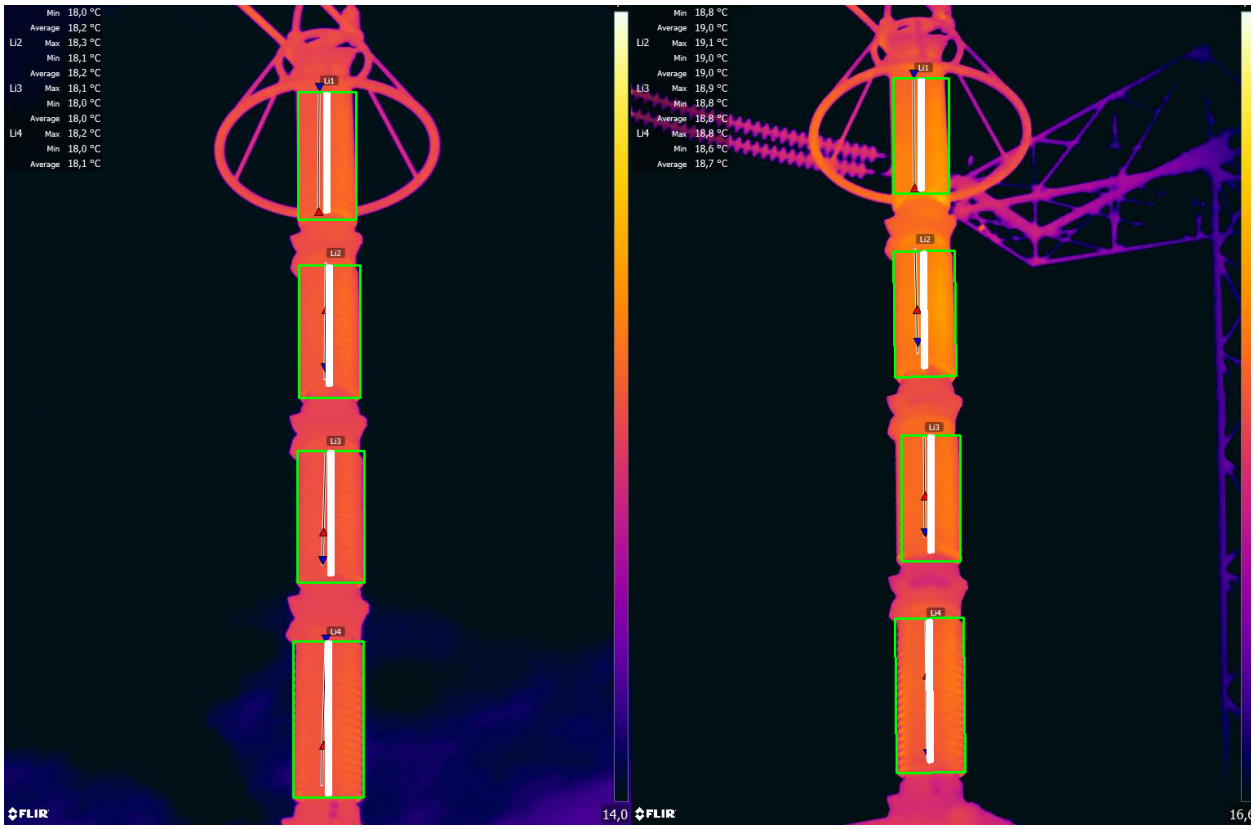

Source: the author, (2023).

A second type of error may arise from undetected segments of the arrester, as demonstrated in **Figure 21**. This issue can be attributed to the model's performance limitations in accurately identifying all segments.

Figure 21 - Undetected arrester sections resulting from the model's limitations.

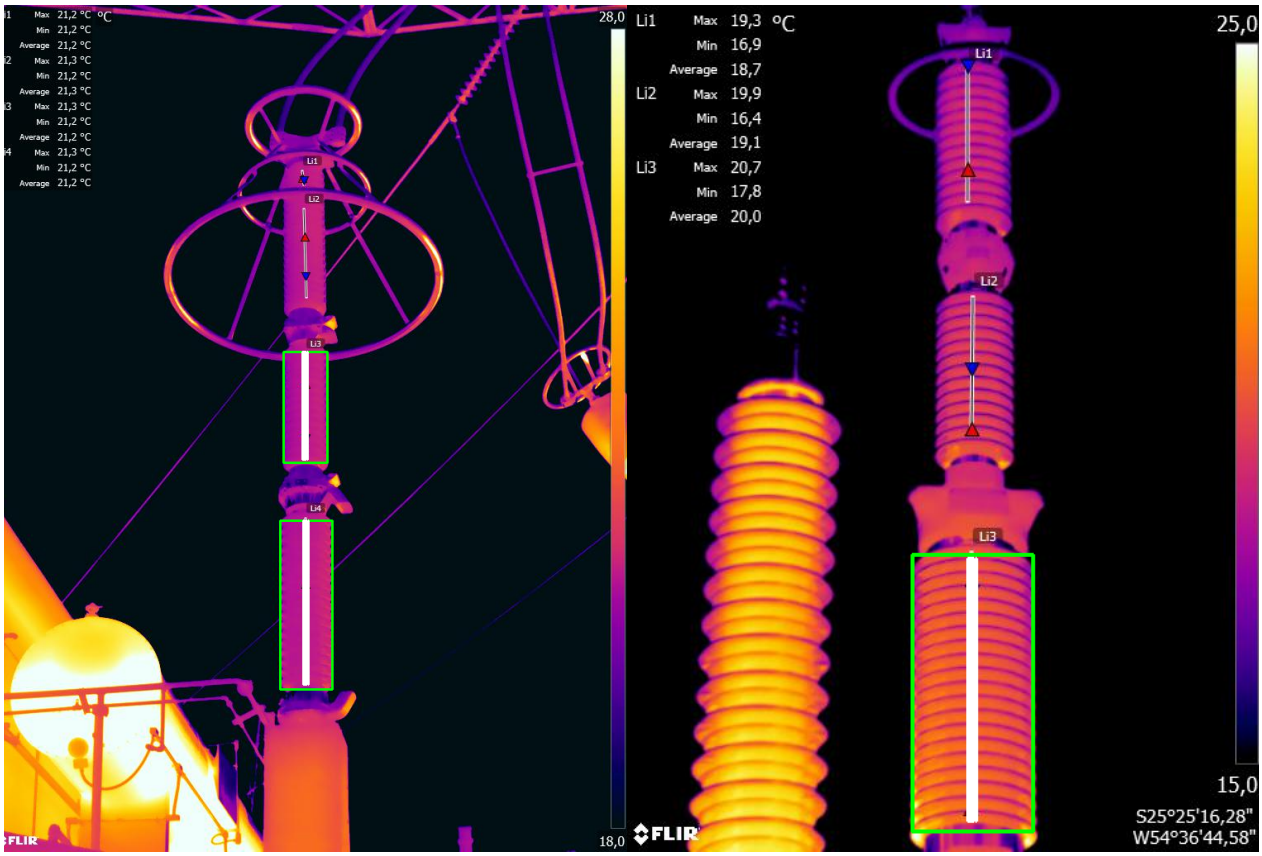

Source: the author, (2023).

To enhance the current method, several approaches can be employed. One option is to disregard the outliers, which constitute approximately 7% of the total observations, and process them manually. The new results are shown in **Table 4** and detailed in **Figure 22**.

Table 4 - Comparison of the automatic to the manual temperature extraction methods before and after disregarding the outliers.

Measurement	MAE (°C)	RMSE (°C)	MAPE (%)
Maximum (with outliers)	0.18	0.50	0.84
Maximum (without outliers)	0.11	0.18	0.54
Average (with outliers)	0.06	0.13	0.43
Average (without outliers)	0.05	0.08	0.38
Delta (with outliers)	0.17	0.46	17.58
Delta (without outliers)	0.10	0.17	11.48

Source: The author, 2023.

Figure 22 - Comparative analysis of temperature measurements after disregarding the outliers.

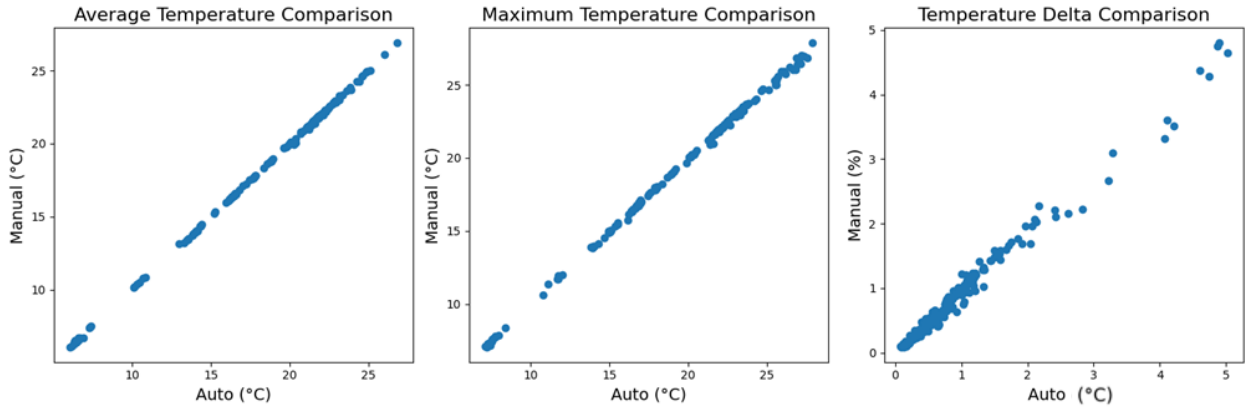

Source: The author, 2023.

In practical applications, the proposed method involves disregarding the outliers by visual inspection and processing them manually to obtain accurate measurements. Therefore, potential enhancements to the method will be addressed in the conclusions section.

The new method we're proposing offers several significant advantages:

- **Automatization**: No need for a specially trained operator to use it, which makes it a more cost-effective choice;
- **Short time**: executes about ten times faster than the manual method, which can save a significant amount of time specially for many images;
- **Reliable**: This method consistently delivers dependable results, making it a trustworthy choice;
- **Open-Source**: This approach utilizes open-source technology, allowing for greater data management autonomy and eliminating the necessity to entrust data to commercial entities.

As well as some disadvantages like:

- **Visual inspection dependence**: Despite its automation, this method necessitates periodic visual checks to guarantee the precision of the results, introducing a degree of manual intervention.

5 CONCLUSIONS

This study aimed to solve a practical problem of manual temperature extraction from lightning arrester's electrical substations. The manual process, often laborious and error-prone, necessitated a more efficient and reliable solution.

To address this, a new method to automatize the temperature extraction process, from thermal image of lightning arresters was proposed and implemented. This method uses Mask R-CNN based deep learning algorithm an image processing to compute the lightning arrester temperature. The proposed and automated method aimed to streamline the temperature extraction process from the thermal images of lighting arresters, enhancing both speed and data reliability. To do this, the original dataset was augmented and split to enable the training and testing of the Mask-R CNN pre-trained model.

The temperature data extracted through the proposed method demonstrated a high level of agreement with those obtained manually, reinforcing the effectiveness of our solution. A similarity analysis with 195 images comparing the manual (original) and automatic (proposed) methods, revealed a Mean Absolute Percentage Error (MAPE) 11.48% for the temperature delta which is the difference between the maximum and average temperature of the arrester.

The proposed method offers significant benefits including automation, eliminating the need for specially trained personnel, making it a cost-effective solution. Moreover, it operates at a speed that significantly outpaces the traditional manual method. Consistency, as it delivers reliable and dependable results. Importantly, this method employs open-source technology, which offers us enhanced control over our data and negates the need to share our data with commercial entities.

One limitation of the current study is the requirement for visual inspection, which introduces potential subjectivity. This is due to the poor handling of a few complex images. Although the algorithm successfully segmented the thermal images, future work should therefore focus on refining the algorithm to minimize this reliance.

Additionally, further improvements may be achieved by annotating more images to enrich and enlarge the training dataset, including the use of cross-validation techniques and hyperparameter tuning, and considering alternative segmentation methods such as Facebook's Segment Anything. Another possible work is creating a user interface or an application programming interface for this tool.

Our study presents a new approach to detect the lightning arrester

degradation from temperature of thermal images. This significant contribution to the field by not only developing an AI-based method for automated temperature extraction, but also providing a comprehensive review of the related scientific literature. We have meticulously detailed the methodology involving the annotation, augmentation, and splitting of data, the training of the Mask R-CNN model, the extraction of temperature data, and the evaluation of the proposed method. Furthermore, we have made the source code available to the scientific community upon request to the author.

Finally, these contributions not only enable the reproducibility of our study but also lay a strong foundation for future work in this domain. The method developed accelerates the diagnosis of lightning arresters at electrical substations, thereby enhancing the efficiency and reliability of this process. Despite the promising results, further advancements are necessary to fully leverage the potential of AI in this domain.

REFERENCES

ABU ALHAIJA, Hassan; KARTHIK MUSTIKOVELA, Siva; MESCHEDER, Lars; GEIGER, Andreas; ROTHER, Carsten. Augmented Reality Meets Deep Learning for Car Instance Segmentation in Urban Scenes. *[S. l.]*, 2017. . Acesso em: 12 abr. 2023.

ALBAWI, Saad; MOHAMMED, Tareq Abed; AL-ZAWI, Saad. Understanding of a convolutional neural network. *Em*: 2017 INTERNATIONAL CONFERENCE ON ENGINEERING AND TECHNOLOGY (ICET) 2017, **Anais** [...]. : IEEE, 2017. p. 1–6. DOI: 10.1109/ICEngTechnol.2017.8308186. Disponível em: https://ieeexplore.ieee.org/document/8308186/. Acesso em: 12 mar. 2023.

ANKRUM, James. Diagnosing skin diseases using an AI-based dermatology consult. **Science Translational Medicine**, *[S. l.]*, v. 12, n. 548, 2020. DOI: 10.1126/SCITRANSLMED.ABC8946. Disponível em: https://www.science.org/doi/10.1126/scitranslmed.abc8946. Acesso em: 8 maio. 2023.

ATTARD, Leanne; DEBONO, Carl James; VALENTINO, Gianluca; DI CASTRO, Mario; MASI, Alessandro; SCIBILE, Luigi. Automatic crack detection using mask R-CNN. **International Symposium on Image and Signal Processing and Analysis, ISPA**, *[S. l.]*, v. 2019- September, p. 152–157, 2019. DOI: 10.1109/ISPA.2019.8868619. Acesso em: 20 abr. 2023.

BHARATI, Puja; PRAMANIK, Ankita. Deep Learning Techniques—R-CNN to Mask R-CNN: A Survey. **Advances in Intelligent Systems and Computing**, *[S. l.]*, v. 999, p. 657–668, 2020. DOI: 10.1007/978-981-13-9042-5_56/COVER. Disponível em: https://link.springer.com/chapter/10.1007/978-981-13-9042-5_56. Acesso em: 12 mar. 2023.

BISONG, Ekaba. Google Colaboratory. **Building Machine Learning and Deep Learning Models on Google Cloud Platform**, *[S. l.]*, p. 59–64, 2019. DOI: 10.1007/978-1-4842-4470-8_7. Disponível em: https://link.springer.com/chapter/10.1007/978-1-4842-4470-8_7. Acesso em: 20 maio. 2023.

BRADSKI, G. The OpenCV Library. **Dr. Dobb's Journal of Software Tools**, *[S. l.]*, 2000.
CEPEL. **CEPEL - Home**. 2023. Disponível em: https://www.cepel.br/. Acesso em: 9 maio. 2023.
COIFMAN, Benjamin; BEYMER, David; MCLAUCHLAN, Philip; MALIK, Jitendra. A real-time computer vision system for vehicle tracking and traffic surveillance. **Transportation Research Part C: Emerging Technologies**, *[S. l.]*, v. 6, n. 4, p. 271–288, 1998. DOI: 10.1016/S0968-090X(98)00019-9. Acesso em: 9 maio. 2023.

CORKE, Peter. **Robotics, Vision and Control**. Berlin, Heidelberg: Springer Berlin Heidelberg, 2011. DOI: 10.1007/978-3-642-20144-8. Disponível em: http://link.springer.com/10.1007/978-3-642-20144-8. Acesso em: 8 maio. 2023.

COSTA, Matheus Souza Teixeira Da; TORRES, Arthur Oliveira Quintão; OLIVEIRA, Leandro Augusto Silva De; ELLER, Weberton Luiz Gonsalves; ROSA, Sérgio Dos Anjos; VALADÃO, Rodrigo Leonardo. Estudo Grupo de Estudo de Subestações e Equipamentos

de Alta Tensão-Gse Diagnóstico Inteligente de Pára-Raios: Uma Nova Abordagem. *Em*: 2019, **Anais** [...]. [s.l: s.n.]. Acesso em: 20 mar. 2023.

FAHIM, Abdullah. **Spatial dissection of a soundfield using spherical harmonic decomposition**. 2020. *[S. l.]*, 2020. Disponível em: https://www.researchgate.net/publication/341520057_Spatial_dissection_of_a_soundfield_using_spherical_harmonic_decomposition. Acesso em: 20 abr. 2023.

FRED AGARAP, Abien M. Deep Learning using Rectified Linear Units (ReLU). *[S. l.]*, 2018. Disponível em: https://arxiv.org/abs/1803.08375v2. Acesso em: 9 maio. 2023.

FRONTIN, Sergio. **Equipamentos De Alta Tensão Prospecção E Hierarquização De Inovações Tecnológicas**. [s.l: s.n.]. . Acesso em: 25 fev. 2023.

GEBRU, Timnit; KRAUSE, Jonathan; WANG, Yilun; CHEN, Duyun; DENG, Jia; AIDEN, Erez Lieberman; FEI-FEI, Li. Using deep learning and Google Street View to estimate the demographic makeup of neighborhoods across the United States. *[S. l.]*, v. 114, p. 13108–13113, 2017. DOI: 10.1073/pnas.1700035114. Acesso em: 8 maio. 2023.

GILL, Paul. **Electrical Power Equipment Maintenance And Testing**. 2. ed. [s.l.] : CRC Press, 2009. . Acesso em: 25 fev. 2023.

GIRSHICK, Ross. Fast R-CNN. **Proceedings of the IEEE International Conference on Computer Vision**, *[S. l.]*, 2015. Disponível em: http://arxiv.org/abs/1504.08083. Acesso em: 9 maio. 2023.

GIRSHICK, Ross; DONAHUE, Jeff; DARRELL, Trevor; MALIK, Jitendra. Rich feature hierarchies for accurate object detection and semantic segmentation. **Proceedings of the IEEE Computer Society Conference on Computer Vision and Pattern Recognition**, *[S. l.]*, p. 580–587, 2013. DOI: 10.1109/CVPR.2014.81. Disponível em: https://arxiv.org/abs/1311.2524v5. Acesso em: 16 abr. 2023.

GVR. **Global Computer Vision Market Size & Share Report, 2030**. 2023. Disponível em: https://www.grandviewresearch.com/industry-analysis/computer-vision-market. Acesso em: 9 maio. 2023.

HAFIZ, Abdul Mueed; BHAT, Ghulam Mohiuddin. A Survey on Instance Segmentation: State of the art. *[S. l.]*, 2020. . Acesso em: 16 mar. 2023.

HE, Kaiming; GKIOXARI, Georgia; DOLLÁR, Piotr; GIRSHICK, Ross. Mask R-CNN. **IEEE Transactions on Pattern Analysis and Machine Intelligence**, *[S. l.]*, v. 42, n. 2, p. 386–397, 2017. DOI: 10.48550/arxiv.1703.06870. Disponível em: https://arxiv.org/abs/1703.06870v3. Acesso em: 12 mar. 2023.

HE, Kaiming; ZHANG, Xiangyu; REN, Shaoqing; SUN, Jian. Deep Residual Learning for Image Recognition. **Proceedings of the IEEE Computer Society Conference on Computer Vision and Pattern Recognition**, *[S. l.]*, v. 2016- December, p. 770–778, 2015. DOI: 10.1109/CVPR.2016.90. Disponível em: https://arxiv.org/abs/1512.03385v1. Acesso em: 16 abr. 2023.

HU, Weiming; TAN, Tieniu; WANG, Liang; MAYBANK, Steve. A survey on visual surveillance of object motion and behaviors. **IEEE Transactions on Systems, Man and Cybernetics Part C: Applications and Reviews**, *[S. l.]*, v. 34, n. 3, p. 334–352, 2004. DOI: 10.1109/TSMCC.2004.829274. Acesso em: 8 maio. 2023.

HUANG, Shyh Jier; HSIEH, Chien Hsien. A method to enhance the predictive maintenance of ZnO arresters in energy systems. **International Journal of Electrical Power & Energy Systems**, *[S. l.]*, v. 62, p. 183–188, 2014. DOI: 10.1016/J.IJEPES.2014.04.041. Acesso em: 19 mar. 2023.

JUNG, Alexander B.; WADA, Kentaro; TANAKA, Satoshi; CRALL, Jon. **imgaug**. 2020. Disponível em: https://github.com/aleju/imgaug. Acesso em: 20 maio. 2023.

KANNAN; NALINI, G. On image segmentation techniques. *[S. l.]*, 2014. . Acesso em: 13 mar. 2023.

KAYALIBAY, Baris; JENSEN, Grady; VAN DER SMAGT, Patrick. CNN-based Segmentation of Medical Imaging Data. *[S. l.]*, 2017. Disponível em: https://arxiv.org/abs/1701.03056v2. Acesso em: 12 abr. 2023.

KIMBALL, Spencer; MATTIS, Peter; NATTERER, Michael; ALANKO, Lauri. **GNU Image Manipulation Program**. 2010. Disponível em: https://www.gimp.org/. Acesso em: 19 abr. 2023.

KIRILLOV, Alexander et al. Segment Anything. *[S. l.]*, 2023. Disponível em: https://segment-anything.com. Acesso em: 9 maio. 2023.

KRIZHEVSKY, Alex; SUTSKEVER, Ilya; HINTON, Geoffrey E. ImageNet Classification with Deep Convolutional Neural Networks. **COMMUNICATIONS OF THE ACM**, *[S. l.]*, v. 60, n. 6, 2017. DOI: 10.1145/3065386. Disponível em: http://code.google.com/p/cuda-convnet/. Acesso em: 9 maio. 2023.

KUMAR, Deepak; KUKREJA, Vinay. Image-Based Wheat Mosaic Virus Detection with Mask-RCNN Model. **2022 International Conference on Decision Aid Sciences and Applications, DASA 2022**, *[S. l.]*, p. 178–182, 2022. DOI: 10.1109/DASA54658.2022.9765199. Acesso em: 20 abr. 2023.

LECUN, Yann; BENGIO, Yoshua; HINTON, Geoffrey. Deep learning. **Nature 2015 521:7553**, *[S. l.]*, v. 521, n. 7553, p. 436–444, 2015. DOI: 10.1038/nature14539. Disponível em: https://www.nature.com/articles/nature14539. Acesso em: 16 abr. 2023.

LIN, Tsung Yi; MAIRE, Michael; BELONGIE, Serge; HAYS, James; PERONA, Pietro; RAMANAN, Deva; DOLLÁR, Piotr; ZITNICK, C. Lawrence. Microsoft COCO: Common Objects in Context. **Lecture Notes in Computer Science (including subseries Lecture Notes in Artificial Intelligence and Lecture Notes in Bioinformatics)**, *[S. l.]*, v. 8693 LNCS, n. PART 5, p. 740–755, 2014. DOI: 10.1007/978-3-319-10602-1_48. Disponível em: https://arxiv.org/abs/1405.0312v3. Acesso em: 13 abr. 2023.

LITJENS, Geert et al. A Survey on Deep Learning in Medical Image Analysis. *[S. l.]*, 2017. . Acesso em: 8 maio. 2023.

MACIEL, Joylan Nunes; WENTZ, Victor Hugo; LEDESMA, Jorge Javier Gimenez; JUNIOR, Oswaldo Hideo Ando. Analysis of Artificial Neural Networks for Forecasting Photovoltaic Energy Generation with Solar Irradiance. **Brazilian Archives of Biology and Technology**, *[S. l.]*, v. 64, n. 21210131, p. 1–14, 2021. DOI: 10.1590/1678-4324-75YEARS-2021210131. Disponível em: http://www.scielo.br/j/babt/a/Qrr9hBPQRb54nTnBQWwwX8c/. Acesso em: 28 ago. 2022.

NAFI'I, Mohammad Wahyudi; YUNIARNO, Eko Mulyanto; AFFANDI, Achmad. Vehicle Brands and Types Detection Using Mask R-CNN. **Proceedings - 2019 International Seminar on Intelligent Technology and Its Application, ISITIA 2019**, *[S. l.]*, p. 422–427, 2019. DOI: 10.1109/ISITIA.2019.8937278. Acesso em: 20 abr. 2023.

OFIR, Nati; NEBEL, Jean-Christophe. Classic versus deep learning approaches to address computer vision challenges. *[S. l.]*, 2021. Disponível em: http://arxiv.org/abs/2101.09744. Acesso em: 13 mar. 2023.

PADILLA, Rafael; NETTO, Sergio L.; DA SILVA, Eduardo A. B. A Survey on Performance Metrics for Object-Detection Algorithms. **International Conference on Systems, Signals, and Image Processing**, *[S. l.]*, v. 2020- July, p. 237–242, 2020. DOI: 10.1109/IWSSIP48289.2020.9145130. Acesso em: 12 maio. 2023.

PEREZ, Luis; WANG, Jason. The Effectiveness of Data Augmentation in Image Classification using Deep Learning. *[S. l.]*, 2017. Disponível em: https://arxiv.org/abs/1712.04621v1. Acesso em: 12 maio. 2023.

POLAT, Enes; MOHAMMED, Hussein Mahmood Abdo; OMEROGLU, Asli Nur; KUMBASAR, Nida; OZBEK, I. Yucel; ORAL, Emin Argun. Multiple Barcode Detection with Mask R-CNN. **2020 28th Signal Processing and Communications Applications Conference, SIU 2020 - Proceedings**, *[S. l.]*, 2020. DOI: 10.1109/SIU49456.2020.9302141. Acesso em: 20 abr. 2023.

REN, Shaoqing; HE, Kaiming; GIRSHICK, Ross; SUN, Jian. Faster R-CNN: Towards Real-Time Object Detection with Region Proposal Networks. **IEEE Transactions on Pattern Analysis and Machine Intelligence**, *[S. l.]*, v. 39, n. 6, p. 1137–1149, 2015. DOI: 10.48550/arxiv.1506.01497. Disponível em: https://arxiv.org/abs/1506.01497v3. Acesso em: 12 mar. 2023.

RUSSELL, Stuart; NORVIG, Peter. **Artificial Intelligence: A Modern Approach**. 3rd edition ed. [s.l.] : Pearson Education, 2016.

WAYMO. **Safety – Waymo**. 2023. Disponível em: https://waymo.com/intl/es/safety/. Acesso em: 8 maio. 2023.

SANTOS, Mario Augusto Caetano Dos. **Diagnóstico De Para-Raios De Óxido De Zinco De Alta Tensão Mediante Emprego De Lógica Paraconsistente Anotada**. 2017. *[S. l.]*, 2017. Acesso em: 26 fev. 2023.

SCHERER, Dominik; MÜLLER, Andreas; BEHNKE, Sven. Evaluation of Pooling Operations in Convolutional Architectures for Object Recognition. **Lecture Notes in**

Computer Science (including subseries Lecture Notes in Artificial Intelligence and Lecture Notes in Bioinformatics), *[S. l.]*, v. 6354 LNCS, n. PART 3, p. 92–101, 2010. DOI: 10.1007/978-3-642-15825-4_10. Acesso em: 9 maio. 2023.

SCHMIDHUBER, Jürgen. Deep learning in neural networks: An overview. **Neural networks : the official journal of the International Neural Network Society**, *[S. l.]*, v. 61, p. 85–117, 2014. DOI: 10.1016/J.NEUNET.2014.09.003. Acesso em: 14 mar. 2023.

SHAFIQ, Muhammad; GU, Zhaoquan; CHEIKHROUHOU, Omar; ALHAKAMI, Wajdi; HAMAM, Habib. The Rise of “internet of Things”: Review and Open Research Issues Related to Detection and Prevention of IoT-Based Security Attacks. **Wireless Communications and Mobile Computing**, *[S. l.]*, v. 2022, 2022. DOI: 10.1155/2022/8669348. Acesso em: 9 maio. 2023.

SILVA FILHO, João Inácio Da. Métodos de Aplicações da Lógica Paraconsistente Anotada de anotação com dois valores - LPA2v. **Seleção Documental: Inteligência Artificial e novas Tecnologias, ISSN 1809-0648, Nº. 1, 2006, págs. 18-25**, *[S. l.]*, n. 1, p. 18–25, 2006. Disponível em: https://dialnet.unirioja.es/servlet/articulo?codigo=2245261&info=resumen&idioma=POR. Acesso em: 2 abr. 2023.

SILVEIRA, James. Modelagem e análise de varistores de óxido metálico de zinco. *[S. l.]*, 2009. Disponível em: https://repositorio.ufsc.br/handle/123456789/93019. Acesso em: 26 fev. 2023.

SIMONYAN, Karen; ZISSERMAN, Andrew. Very Deep Convolutional Networks for Large-Scale Image Recognition. **3rd International Conference on Learning Representations, ICLR 2015 - Conference Track Proceedings**, *[S. l.]*, 2014. Disponível em: https://arxiv.org/abs/1409.1556v6. Acesso em: 16 abr. 2023.

SZELISKI, Richard. Computer Vision. Texts in Computer Science. Cham, Texts in Computer Science, 2022. DOI: 10.1007/978-3-030-34372-9. Disponível em: https://link.springer.com/10.1007/978-3-030-34372-9. Acesso em: 8 maio. 2023.

TAIGMAN, Yaniv; YANG, Ming; RANZATO, Marc’Aurelio; WOLF, Lior. DeepFace: Closing the gap to human-level performance in face verification. **Proceedings of the IEEE Computer Society Conference on Computer Vision and Pattern Recognition**, *[S. l.]*, p. 1701–1708, 2014. DOI: 10.1109/CVPR.2014.220. Acesso em: 8 maio. 2023.

TELEDYNE. **FLIR Tools**. 2023a. Disponível em: https://flir-br.custhelp.com/app/answers/detail/a_id/1453/~/download-flir-tools. Acesso em: 30 abr. 2023.

TELEDYNE. **FLIR Science SDK**. 2023b. Disponível em: https://www.flir.com/products/flir-science-file-sdk/?vertical=rd+science&segment=solutions. Acesso em: 30 abr. 2023.

TELEDYNE. **FLIR T660**. 2023c. Disponível em: https://inte.flir.com.br/products/t660/?vertical=condition+monitoring&segment=solutions. Acesso em: 9 maio. 2023.

UIJLINGS, J. R. R.; VAN DE SANDE, K. E. A.; GEVERS, T.; SMEULDERS, A. W. M. Selective search for object recognition. **International Journal of Computer Vision**, *[S. l.]*, v. 104, n. 2, p. 154–171, 2013. DOI: 10.1007/S11263-013-0620-5/METRICS. Disponível em: https://link.springer.com/article/10.1007/s11263-013-0620-5. Acesso em: 10 maio. 2023.

VOULODIMOS, Athanasios; DOULAMIS, Nikolaos; DOULAMIS, Anastasios; PROTOPAPADAKIS, Eftychios. Deep Learning for Computer Vision: A Brief Review. **Computational Intelligence and Neuroscience**, *[S. l.]*, 2018. DOI: 10.1155/2018/7068349. Acesso em: 13 mar. 2023.

WEISS, Karl; KHOSHGOFTAAR, Taghi M.; WANG, Ding Ding. A survey of transfer learning. **Journal of Big Data**, *[S. l.]*, v. 3, n. 1, p. 1–40, 2016. DOI: 10.1186/S40537-016-0043-6/TABLES/6. Disponível em: https://journalofbigdata.springeropen.com/articles/10.1186/s40537-016-0043-6. Acesso em: 30 abr. 2023.

WU, Yuxin; KIRILLOV, Alexander; MASSA, Francisco; GIRSHICK, Ross. **Detectron2**. 2019a. Disponível em: https://github.com/facebookresearch/detectron2. Acesso em: 20 maio. 2023.

WU, Yuxin; KIRILLOV, Alexander; MASSA, Francisco; GIRSHICK, Ross. **Detectron2 Model**. , 2019. b. Disponível em: https://github.com/facebookresearch/detectron2/blob/main/configs/COCO-InstanceSegmentation/mask_rcnn_R_50_FPN_3x.yaml. Acesso em: 20 maio. 2023.

YAHUI PENG; XIAOCHEN LIU; CHONG SHEN; HAOQIAN HUANG. An Improved Optical Flow Algorithm Based on Mask-R-CNN and K-Means for Velocity Calculation. **applied sciences**, *[S. l.]*, 2019. Disponível em: https://www.researchgate.net/publication/334460507_An_Improved_Optical_Flow_Algorithm_Based_on_Mask-R-CNN_and_K-Means_for_Velocity_Calculation. Acesso em: 20 abr. 2023.

YEGNANARAYANA, Bayya. **Artificial neural networks**. [s.l.] : PHI Learning Pvt. Ltd., 2009.

ZHANG, Qinghui; CHANG, Xianing; BIAN, Shanfeng Bian. Vehicle-Damage-Detection Segmentation Algorithm Based on Improved Mask RCNN. **IEEE Access**, *[S. l.]*, v. 8, p. 6997–7004, 2020. DOI: 10.1109/ACCESS.2020.2964055. Acesso em: 20 abr. 2023.

ZOU, Zhengxia; CHEN, Keyan; SHI, Zhenwei; GUO, Yuhong; YE, Jieping. Object Detection in 20 Years: A Survey. **Proceedings of the IEEE**, *[S. l.]*, 2023. DOI: 10.1109/JPROC.2023.3238524. Acesso em: 16 abr. 2023.